

1 **A year in the life of the Eastern Mediterranean:**

2 **Monthly dynamics of phytoplankton and bacterioplankton in an ultra-oligotrophic sea**

3

4 Tom Reich¹, Tal Ben-Ezra^{1,2}, Natalya Belkin³, Anat Tsemel^{1,2}, Dikla Aharonovich¹, Dalit

5 Roth-Rosenberg¹, Shira Givati¹, Or Bialik⁴, Barak Herut^{3,4}, Ilana Berman-Frank¹, Miguel

6 Frada^{5,6}, Michael D. Krom^{1,2}, Yoav Lehahn⁴, Eyal Rahav^{3*} and Daniel Sher^{1*}

7

8 ¹Department of Marine Biology, Leon H. Charney School of Marine Sciences, University of

9 Haifa, Israel; ²Morris Kahn Marine Research Station, Leon H. Charney School of Marine

10 Science, University of Haifa, Haifa, 3498838, Israel. ³Israel Oceanographic and Limnological

11 Research, Haifa, Israel. ⁴Department of Maritime Geosciences, Leon H. Charney School of

12 Marine Sciences, University of Haifa, Israel. ⁵The Interuniversity Institute for Marine

13 Sciences in Eilat, POB 469, 88103 Eilat, Israel. ⁶Dept. of Ecology, Evolution and Behavior –

14 Alexander Silberman Institute of Life Sciences, Hebrew University of Jerusalem, Jerusalem

15 91904, Israel

16

17 *Corresponding authors:

18 dscher@univ.haifa.ac.il

19 eyal.rahav@ocean.org.il

20

21 **Keywords:** Eastern Mediterranean, Levantine Basin, seasonal dynamics, primary

22 productivity, bacterial productivity, phytoplankton, *Prochlorococcus*, *Synechococcus*, pico-
23 eukaryotes.

24 **Highlights**

25 • Bacterioplankton dynamics were assessed monthly in the Eastern Mediterranean Sea

26 • Small-sized picophytoplankton numerically dominated the phytoplankton community

27 • Seasonal phytoplankton dynamics are similar to BATS and Red Sea, but not to HOT

28 • Annual primary productivity is among the lowest in the world's oceans

29 • Bacterial to primary production ratio is higher than most oligotrophic seas

30 **Abstract**

31 The Eastern Mediterranean Sea (EMS) is a poorly studied ultra-oligotrophic marine
32 environment, dominated by small-size phyto- and bacterioplankton. Here, we describe the
33 dynamics of a single annual cycle (2018-19) of phyto- and bacterioplankton (abundances,
34 pigments and productivity) in relation to the physical and chemical conditions in the photic
35 water column at an offshore EMS site (Station THEMO-2, ~1,500m depth, 50km offshore).
36 We show that phytoplankton biomass (as chlorophyll a), primary and bacterial productivity
37 differed between the mixed winter (January-April) and the thermally stratified (May-
38 December) periods. *Prochlorococcus* and *Synechococcus* numerically dominated the
39 picophytoplankton populations, with each clade revealing different temporal and depth
40 changes indicative to them, while pico-eukaryotes (primarily haptophytes) were less
41 abundant, yet likely contributed significant biomass. Estimated primary productivity (~32 gC
42 m⁻² y⁻¹) was lower compared with other well-studied oligotrophic locations, including the
43 north Atlantic and Pacific (BATS and HOT observatories), the western Mediterranean
44 (DYFAMED observatory) and the Red Sea, and was on-par with the ultra-oligotrophic South
45 Pacific Gyre. In contrast, integrated bacterial production (~11 gC m⁻² y⁻¹) was similar to other
46 oligotrophic locations. Phytoplankton seasonal dynamics were similar to those at BATS and
47 the Red Sea, suggesting an observable effect of winter mixing in this ultra-oligotrophic
48 location. These results highlight the ultra-oligotrophic conditions in the EMS and provide, for
49 the first time in this region, a full-year baseline and context to ocean observatories in the
50 region.

51 **1 Introduction**

52

53 Convective mixing of the water column is one of the main mechanisms responsible
54 for transport of nutrients to the photic zone of oligotrophic oceans and seas, often resulting in
55 increased phytoplankton biomass and activity (Behrenfeld, 2010). This process usually
56 occurs during wintertime upon the progressive cooling of the sea surface, although other
57 mechanisms may also deliver nutrients to the mixed layer such as physical upwelling along
58 shorelines, frontal systems and gyres (Anabalón et al., 2016), nutrient runoff from rivers
59 (Jickells, 1998), and atmospheric deposition (Guieu et al., 2014). Stratification is established
60 during springtime, nutrients gradually become depleted, which, together with other processes
61 such as increased predation, lead to a decline in algal biomass and productivity (Behrenfeld
62 and Boss, 2014). This cycle has been extensively studied over decades in the major
63 oligotrophic gyres (e.g. HOT and BATS) (Steinberg et al., 2001), as well in other locations
64 including the Western Mediterranean and Red Seas (Genin et al., 2018; Marty et al., 2002;
65 Marty and Chiavérini, 2010), and is considered a fundamental driving force of marine
66 ecosystem structure and function.

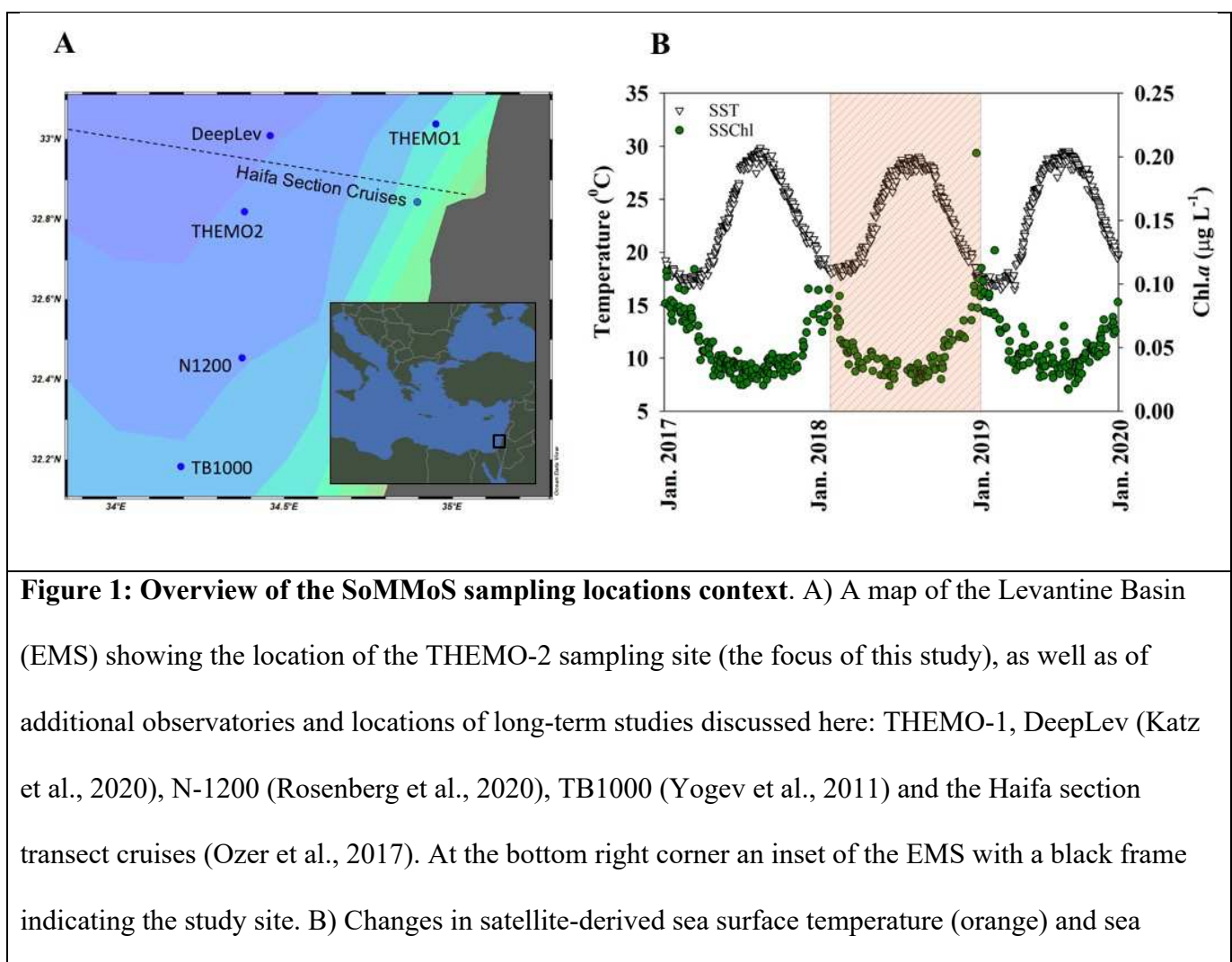
67 The offshore water of the Eastern Mediterranean Sea are considered ultra-oligotrophic
68 (Berman-Frank and Rahav, 2012; Siokou-Frangou et al., 2010). The oligotrophic nature of
69 this system, and especially of the Eastern Mediterranean Sea (EMS), is mainly driven by its
70 general anti-estuarine circulation (Pinardi and Masetti, 2000). Additionally, the relatively
71 stable density stratification throughout most of the year (winter mixing rarely exceeds the 200
72 m depth, (D'Ortenzio et al., 2005) has been suggested to result in a very low supply of deep
73 water nutrients to the euphotic zone (Hazan et al., 2018). Finally, modern riverine inputs into
74 the EMS are extremely low, especially since the Nile was dammed in the 1960s (Krom et al.,
75 2014). The abovementioned conditions makes the EMS, and specifically the easternmost

76 Levantine basin, among the warmest, saltiest and least productive waters in the world (Ozer
77 et al., 2017).

78 Despite the importance of the EMS coastline in providing ecosystem services to over 70
79 million people e.g. (Peled et al., 2018), it lacks the continued high resolution records
80 available from other oligotrophic regions such as the North Atlantic (the Bermuda Atlantic
81 Time Series, BATS), North Pacific (The Hawaii Ocean Time-Series station ALOHA, HOT),
82 the Western Mediterranean e.g. station DYFAMED (Marty et al., 2002; Marty and
83 Chiavérini, 2010) and, to a lesser extent, the Red Sea (Shaked and Genin, 2017). Specifically,
84 detailed phytoplankton and bacterioplankton time-series are missing, and are important in
85 order to both understand the current system and the ways it may be impacted by local,
86 regional and global change (e.g. (Marty and Chiavérini, 2010). Thus, studying the dynamics
87 of the microorganisms at the base of the marine food-web over time are of great ecological
88 importance.

89 Studies from the early 1980's showed a clear seasonal cycle of chlorophyll a (a proxy of algal
90 biomass) and primary production in surface waters of both neritic and pelagic locations, with
91 the changes attributed primarily to picophytoplankton (Azov, 1986; Berman et al., 1984;
92 Kimor and Wood, 1975; Yacobi et al., 1995). More recent studies of the EMS show similar
93 seasonal trends using remote-sensing of surface chlorophyll a (Rosenberg et al., 2020) and in
94 measurements of cell numbers, production and dinitrogen fixation in coastal waters (Rahav et
95 al., 2018; Raveh et al., 2015). However, to the best of our knowledge, no detailed temporal
96 (monthly) measurements have been presented of microbial processes and phytoplankton
97 community structure at the offshore EMS waters. In this study, we followed the composition
98 and activity of phytoplankton and bacterioplankton from a pelagic location (station THEMO-
99 2) in the offshore EMS over a full year at monthly temporal resolution, and at high depth
100 resolution (~20 samples, ~12 of them across the photic zone). These measurements were

101 performed as part of the SoMMoS (Southeastern Mediterranean Monthly cruise Series)
102 campaign, which compared an open-ocean station with one at the edge of the continental
103 shelf (Figure 1A). Additional studies from this cruise series will focus on the carbonate
104 system (Juntao et al. *in prep*), nutrient dynamics (Ben Ezra et al., 2021), coccolithophore
105 dynamics (Keuter et al. *in prep*) and a detailed comparison of the offshore and coastal
106 stations (Krom et al. *in prep*). Together, these studies provide a baseline allowing improved
107 interpretation for future research from the two long-term ocean observatories recently
108 established in the EMS: the DeepLev (Katz et al., 2020) and THEMO (Diamant et al., 2020),
109 as well as comparison to long-term monitoring activities (Ozer et al., 2017; Rahav et al.,
110 2019; Sisma-Ventura et al., 2021).



surface chlorophyll a (green) from the 1 km² region surrounding THEMO-2 between 2017-2020. Data were extracted from the Copernicus Marine Environment Monitoring Service (CMEMS, <https://marine.copernicus.eu/>). The period of this study is shaded.

111

112 **2 Materials and Methods**

113 **2.1 Cruises and sample collection**

114 Water samples were collected as part of the SoMMoS project during twelve cruises, from
115 February 2018 until January 2019. Each cruise took samples at two stations: THEMO2, an
116 open ocean station at a depth of ~1500 m (~50 Km from the coast, 32.820 N, 34.380 E), and
117 THEMO1 which is positioned at the edge of the continental shelf at ~125m depth (~10 Km
118 from the coast, 33.040 N, 34.950 E). THEMO2 was sampled from 12:00-22:00 (local time),
119 while THEMO1 was sampled during the night, typically 00:00-02:00 (local time). Here, we
120 will present information from data collected at the offshore THEMO2 station. Samples were
121 collected using a 12-bottle rosette with 8 L Niskin bottles. Samples were collected at 20-24
122 depths across the entire water column (11-12 bottles between the surface and 200 m, which
123 we define here as the photic zone). Sampling depths were selected based on real-time data of
124 Conductivity, Temperature, Depth (CTD) profiler (Seabird 19 Plus) from the down-cast
125 before each sample collection in the up-cast, an oxygen optode (on some cruises) and a
126 fluorescence meter (Turner designs, Cyclops-7). The continuous data was processed using the
127 Sea-Bird data conversion software, and minimized using bin averaging. One bin of data lines
128 was defined as a change of 1 decibar (db) between each bin. The first two meters of
129 measurements were compiled together to account for sensors and CTD pump adjustment time
130 and rosette depth while at sea surface. Each cast allocated water for analysis in the following
131 order to give priority to the more ‘sensitive’ parameters: dissolved methane, pH, alkalinity,
132 dissolved inorganic carbon, inorganic nutrients, total and dissolved organic carbon, cell

133 count, primary and bacterial production, DNA and algal pigment markers. Pre-filtered
134 inorganic nutrient samples were analyzed fresh (unfrozen) the day after the cruise, using a
135 SEAL AA-3 autoanalyzer system, and are described in detail elsewhere (Ben-Ezra et al.,
136 2021). A summary of all of the currently-available measurements can be found in
137 Supplementary Table S1, and the BCO-DMO (acronym: SoMMoS) and ISRAMAR
138 (<https://isramar.ocean.org.il/isramar2009/>) databases. Mixed layer depth (MLD) was
139 calculated using a temperature difference of $\Delta 0.3$ °C (Mena et al., 2019). Calculations based
140 on a density difference of $\Delta 0.15$ kg/m³ yielded similar results. During several months
141 (February-April 2018 and January 2019), the density plots revealed a progressive increase in
142 density without a clear pycnocline but with multiple “bumps”, indicative of water column
143 instability down to below 200 m (Supplementary Figure S1). At these times, the MLD
144 calculations based on a defined difference in temperature or salinity from the surface
145 preclude a robust estimate of the mixed layer depth, as they may underestimate the actual
146 values. Based on these calculations, we divide the study period into ‘a generally mixed
147 period’ during January-April (winter/spring), and a ‘stratified period’ during May-December
148 (summer/autumn, Table 1). Estimates based on the vertical distribution of inorganic nutrient
149 concentrations suggest the mixing period may have begun as early as November 2018 (Ben-
150 Ezra et al., 2021). We note that the monthly sampling resolution likely to ‘miss’ short-lived
151 deep mixing events, as can be observed from mooring operations (e.g. (Gunn et al., 2020)).
152

153 **2.2 Bacterial and primary productivity**

154 Heterotrophic prokaryotic productivity (hereafter referred to as bacterial productivity, BP)
155 was estimated using the ³H-leucine incorporation method (Simon and Azam, 1989).
156 Triplicate 1.7 ml of ocean water were taken from each sampled depth and incubated with a
157 7:1 mixture of ‘cold’ leucine and ‘hot’ ³H-leucine (final concentration 100 nmol leucine L⁻¹)

158 for 4 h at room temperature in the dark immediately after sampling. Preliminary experiments
159 show that this was a saturating level of leucine in the offshore water of the SE Mediterranean
160 Sea. After incubation, incorporation was terminated by adding 100 μ l trichloroacetic acid
161 (TCA). As a negative control for non-specific binding, another set of triplicates were sampled
162 from a surface layer and treated with TCA immediately after the addition of the radioactive
163 tracer. At the end of each cruise, the samples were processes using the micro-centrifugation
164 protocol and 1ml scintillation cocktail (ULTIMA-GOLD) was added to all samples before
165 counted using TRI-CARB 2100 TR (PACKARD) scintillation counter. A conversion factor
166 of 3 kg C per mole of leucine incorporated and an isotopic dilution of 2.0 were used to
167 calculate the C incorporated (Simon and Azam, 1989).

168 Net daily photosynthetic carbon fixation rates were estimated using the ^{14}C incorporation
169 method (Nielsen, 1952), with several modifications (Hazan et al., 2018). Triplicate 50 ml
170 samples were taken from each depth within the photic zone and from one aphotic depth using
171 sterile vials and kept at surface light and temperature conditions. The ‘dark’ sample served as
172 blank and was kept under the same temperature as the ‘light’ samples. Radioactive spiking
173 was done at ~08:00 AM the day following of the cruise in order to start a 24h incubation for
174 all samples (including those collected at THEMO-1 station, not shown) at the same time.

175 Early work by Letelier and colleagues (1996) at station HOT showed that prolonged on-deck
176 incubations, similarly to the protocol used in this study, may result in underestimated PP rates
177 as it cannot precisely mimic the temperature and illumination levels in-situ. Our preliminary
178 tests concur with this conclusion and found that ashore incubations underestimate PP rates by
179 up to ~20% compared to incubations onto a mooring rope tied to the ship (Figure S2).

180 Samples were spiked with 50 μ l (5 μCi) of $\text{NaH}^{14}\text{CO}_3$ tracer and were incubated for 24 h
181 under 3 light regimes: surface illumination (samples from the upper mixing depths), 50%
182 illumination (samples from below the mixing depth to the DCM) and ~1% illumination

183 (samples from the DCM and below). Shading was performed using neutral density nets, thus
184 changing light intensity but not spectral properties. Water samples were then filtered through
185 GF/F filters (0.7 μm nominal pore size, 25 mm diameter) using low vacuum pressure (< 50
186 mmHg) and rinsed 3 times with filtered sea water. Filters from each sample were then put in
187 scintillation vials where 50 μl of 32%HCl solution was immediately added in order to remove
188 excess ^{14}C -bicarbonate and kept overnight for incubation. After incubation 5 mL scintillation
189 cocktail (ULTIMA-GOLD) was added to the samples and counted using TRI-CARB 2100
190 TR (PACKARD) scintillation counter. Three random aliquots were counted immediately
191 after the addition of the radiotracer (without incubation) with ethanolamine to serve as added
192 activity measurements.

193

194 **2.3 Picophytoplankton abundance using flow-cytometry**

195 Triplicates water samples (1.5 ml) were collected from each sampling depth, put in cryo-vials
196 (Nunc), and supplemented with 7.5 μl 25% glutaraldehyde (Sigma). Vials were incubated in
197 the dark for 10 min, flash-frozen in liquid nitrogen, and stored in -80 °C freezer. Before
198 analysis, samples were thawed in the dark at room temperature. Each sample was run twice
199 on a BD Canto II flow-cytometer with 2 μm diameter fluorescent beads (Polysciences,
200 Warminster, PA, USA) as a size and fluorescence standard. In the first run three types of
201 phytoplankton cells were identified based on their natural auto-fluorescence:
202 *Prochlorococcus*, *Synechococcus* and picoeukaryotes. Cells were differentiated based on cell
203 chlorophyll (Ex482nm/Em676nm, PerCP channel) and phycoerythrin fluorescence
204 (Ex564nm/Em574nm), and by the size of cell (forward scatter). Before the second FCM, run
205 samples were stained with SYBR Green I (Molecular Probes/ ThermoFisher) to enable
206 counting followed by detection at Ex494nm/Em520nm (FITC channel). This provided counts
207 of the total bacterial population (phytoplankton + heterotrophic bacteria and archaea) as well

208 as a distinction between cells with High or Low DNA content (not shown). Data were
209 processed using FlowJo software. Flow rates were determined several times during each
210 running session by weighing tubes with double-distilled water, and counts of the standard
211 beads were used to verify a consistent flow rate.

212

213 **2.4 Algal pigment markers**

214 Eight litters of seawater were collected from all photic sample depths and one from a dark
215 depth (depth varies between cruises). Water was filtered onto GF/F filters (0.7 μ m nominal
216 pore size, 47mm diameter, Waters) using a peristaltic pump until either all 8 L were filtered
217 or the filter became blocked, in which case the volume filtered was recorded. Filters were
218 placed in cryo-vials and flash frozen in liquid nitrogen until they could be stored in a -80 $^{\circ}$ C
219 freezer. Pigments were extracted in 1ml 100% methanol for 3 h at room temperature and
220 clarified using syringe filters (Acrodisc CR, 13 mm, 0.2 μ m PTFE membranes, Pall Life
221 Sciences). Total chlorophyll was measured spectrophotometrically using a NanoDrop 2000c
222 (Thermo Sciences) at 632, 652, 665 and 695 nm, and the concentration of chlorophyll a was
223 calculated (Ritchie 2008). Ultra high-pressure Liquid Chromatography (UPLC) was
224 performed on an ACQUITY UPLC system (Waters) equipped with a photodiode array
225 detector. A C8 column (1.7 μ m particle size, 2.1 mm internal diameter, 50 mm column
226 length, ACQUITY UPLC BEH, 186002877) was used. The chromatography method was
227 adapted for UPLC from the LOV method (Hooker et al., 2005). Samples were preheated to
228 30 $^{\circ}$ C and column to 50 $^{\circ}$ C before each run. Running buffers were a 70:30 mixture of
229 methanol and 0.5M ammonium acetate (buffer A) and 100% methanol (buffer B). The
230 program consisted of an isocratic run using a 80:20 mixture of buffers A:B for 2min,
231 followed by a linear gradient to 50:50 for 7 minutes and an increase to 100% solvent B. The
232 flow rate was 0.5ml/min. Pigment standards from DHI (Denmark) were used to identify the

233 UPLC peaks (chlorophyll a, divinyl-chlorophyll a, chlorophyll b, chlorophyll c2, zeaxanthin,
234 beta-carotene, diatoxanthin, fucoxanthin, peridinin, 19'- butanoyloxyfucoxanthin and 19'-
235 hexanoyloxyfucoxanthin). Due to potential degradation of the pigment standards, we present
236 the total chlorophyll measured spectrophotometrically and the pigment ratios within each
237 UPLC run.

238

239 **3 Results**

240 **3.1 Physical and chemical properties of the water column**

241 Between January 2016 and December 2019, a clear pattern was observed in satellite-derived
242 sea surface temperature at the THEMO-2 location (Figure 1B), which was mirrored during
243 the monthly cruise measurements (February 2018-January 2019, Figure 2A). The measured
244 *in-situ* sea surface temperatures increased by > 11 °C from the winter minimum of ~17.9 °C to
245 the summer maximum of 29.1 °C (Figure 2A, Supplementary Figure S3, Table 1). Sea
246 surface salinity also increased from a winter minimum of ~39.3 psu to a summer maximum
247 of 39.8 psu (Figure 2B, Supplementary Figure S3). Both temperature and salinity minima
248 were higher than the climatological minima (~15.2 °C and 38.9 psu, measured between 2002-
249 2020 (Herut et al., 2020), suggesting that the sampling period represents a relatively warm
250 and salty year. The temporal changes in sea surface temperature and salinity led to
251 differences in the water density profiles (Figure S1), indicative of stratification of the upper
252 water layer between May and December 2018 (Mixed Layer Depth = 15-49 m) and mixed
253 between February-April 2018 and January 2019 (MLD not determined, see materials and
254 methods) (Table 1). Inorganic nutrient ($\text{NO}_3 + \text{NO}_2$) concentrations began to increase in the
255 mixed layer already during November, suggesting that the stratification had started to erode
256 earlier than observed based on the density profiles, possibly due to short-term mixing events
257 (e.g. (Gunn et al., 2020).

258 Dissolved oxygen concentrations were at or above 100% saturation throughout the whole
259 photic layer (0-200 m), ranging from $\sim 180 \mu\text{mol L}^{-1}$ to $\sim 240 \mu\text{mol L}^{-1}$ (Figure 2C). Where,
260 soluble reactive phosphorus (SRP) concentrations at the surface water were at or close to the
261 limit of detection $\sim 0.006 \mu\text{M}$, ($\sim 6 \text{nM}$) throughout the year, whereas nitrate+nitrite (NOx)
262 were close to the detection limits from August to November (limit of detection $0.013 \mu\text{M}$) but
263 reached $0.3\text{-}0.5 \mu\text{M}$ during the mixed period (Table 1, and see Ben Ezra et al., 2021 for more
264 information).

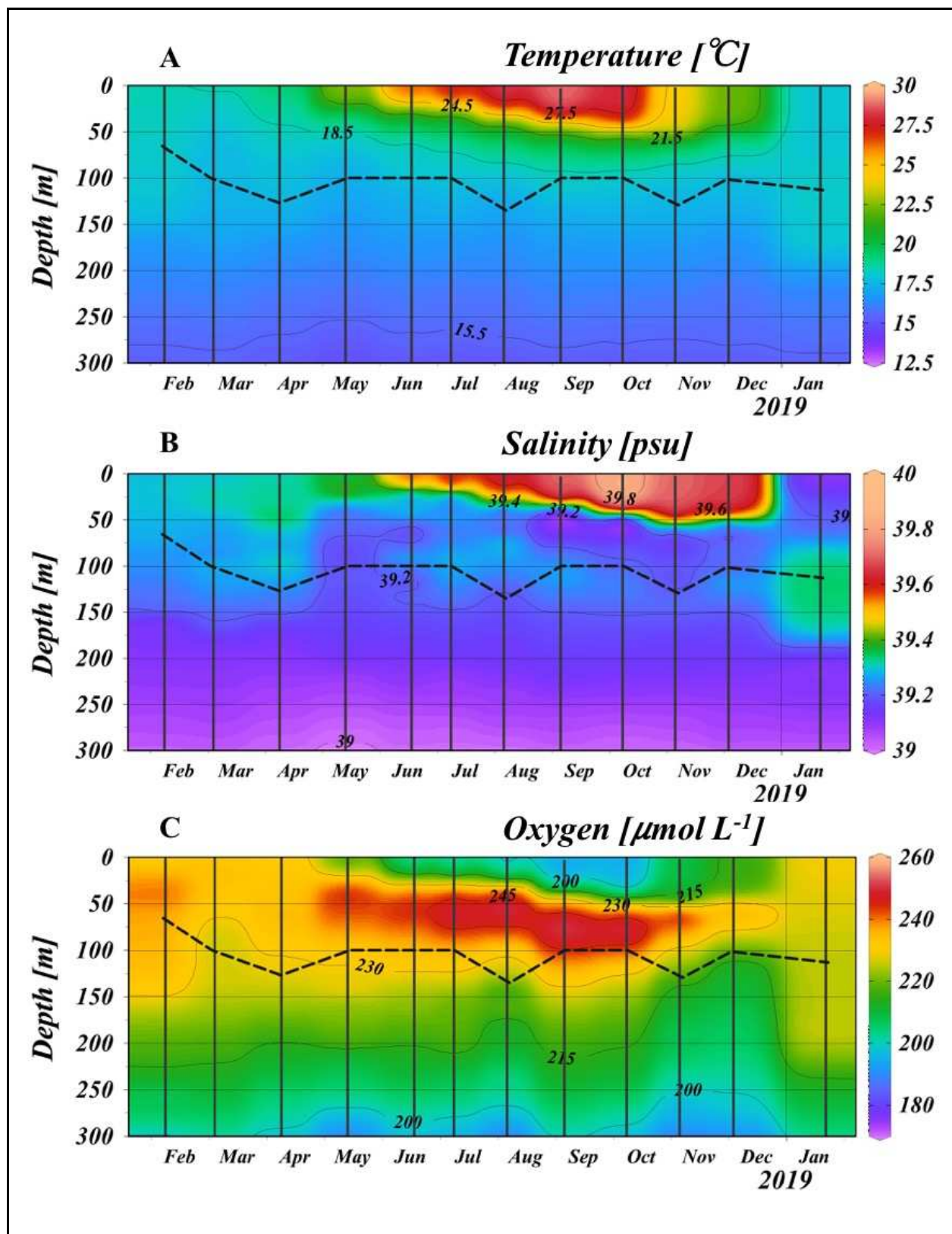


Figure 2: Temperature (A), Salinity (B) and oxygen concentrations (C) at THEMO2 station measured monthly between February 2018 to January 2019. The dashed line represents the depth of the Deep Chlorophyll Maximum (DCM). See Supplementary Figure S3 for the full depth profiles to ~1,400m.

265

266 **Table 1:** Median and range of major measured oceanographic parameters during the mixed
267 and stratified periods. BDL – Below detection limit. ND – not determined (see materials and
268 methods and Supplementary Figure S1 for details). Depth-integrated values are from 0-200m.

Parameter	Mixed period (Jan-Apr)	Thermally Stratified period (May-Dec)
SST (°C)	18.6 (17.9-19.6)	24.2 (22.1-29.1)
Mixed layer depth (m)	ND	26.5 (15-49)
DCM depth (m)	105 (67-125)	100 (100-135)
Surface (10 m) PO ₄ [μM]	BDL (\leq 0.006)	BDL (\leq 0.006)
Surface (10 m) NO _x [μM]	0.3 (0.3-0.6)	0.1 (0.03-0.5)
Surface Si [μM]	0.8 (0.8-1)	0.7 (0.6-1)
Chl <i>a</i> [mg m ⁻²]	14.6 (8.6-17.8)	8.8 (5.4-24.6)
<i>Synechococcus</i> [cells m ⁻²]	1×10^{12} (5.8×10^{11} - 1.6×10^{12})	5×10^{11} (5×10^{10} - 8.5×10^{11})
<i>Prochlorococcus</i> [cells m ⁻²]	7.1×10^{11} (2.5×10^{11} - 2.2×10^{12})	2.3×10^{12} (1×10^{12} - 3.2×10^{12})
Pico-eukaryotes [cells m ⁻²]	1.7×10^{11} (BDL- 7.67×10^{11})	8.6×10^9 (7.2×10^7 - 2.3×10^{11})
Heterotrophic prokaryotes [cells m ⁻²]	6.6×10^{13} (6×10^{13} - 1.03×10^{14})	5.4×10^{13} (3.1×10^{13} - 1.1×10^{14})
PP [mgC m ⁻² d ⁻¹]	113 (69-142)	60 (48-111)
BP [mgC m ⁻² d ⁻¹]	54 (32-71)	18 (7-27)

269

270 **3.2 Chlorophyll a, Primary Productivity and Bacterial Productivity**

271 While satellite-derived sea surface chlorophyll *a* showed a clear seasonal cycle over three
272 years, with lower levels during the stratified period (Figure 1B), the entire photic zone
273 displayed more complex evolution in depth and chlorophyll concentrations (Figure 3A, B). A
274 prominent Deep Chlorophyll Maximum (DCM) was observed year-round, ranging from
275 depths of 60 m (February 2019) to 120 m (April 2019). The concentration of total
276 chlorophyll *a* at the DCM was always higher than that measured at the surface, and ranged
277 between $\sim 0.15 \mu\text{g L}^{-1}$ during February-July, decreasing to $\sim 0.07 \mu\text{g L}^{-1}$ during August-
278 November. These values are within the range or somewhat lower than those measured in
279 other studies in the EMS (~ 0.09 - $0.42 \mu\text{g L}^{-1}$) (Christaki et al., 2001; Yacobi et al., 1995), and
280 are ~ 50 - 80% lower than at BATS (Steinberg et al., 2001). Due primarily to the changes in
281 chlorophyll *a* at the DCM, the integrated chlorophyll did not follow the same temporal
282 variability as observed with the sea-surface satellites measurements (Figure 1B).

283

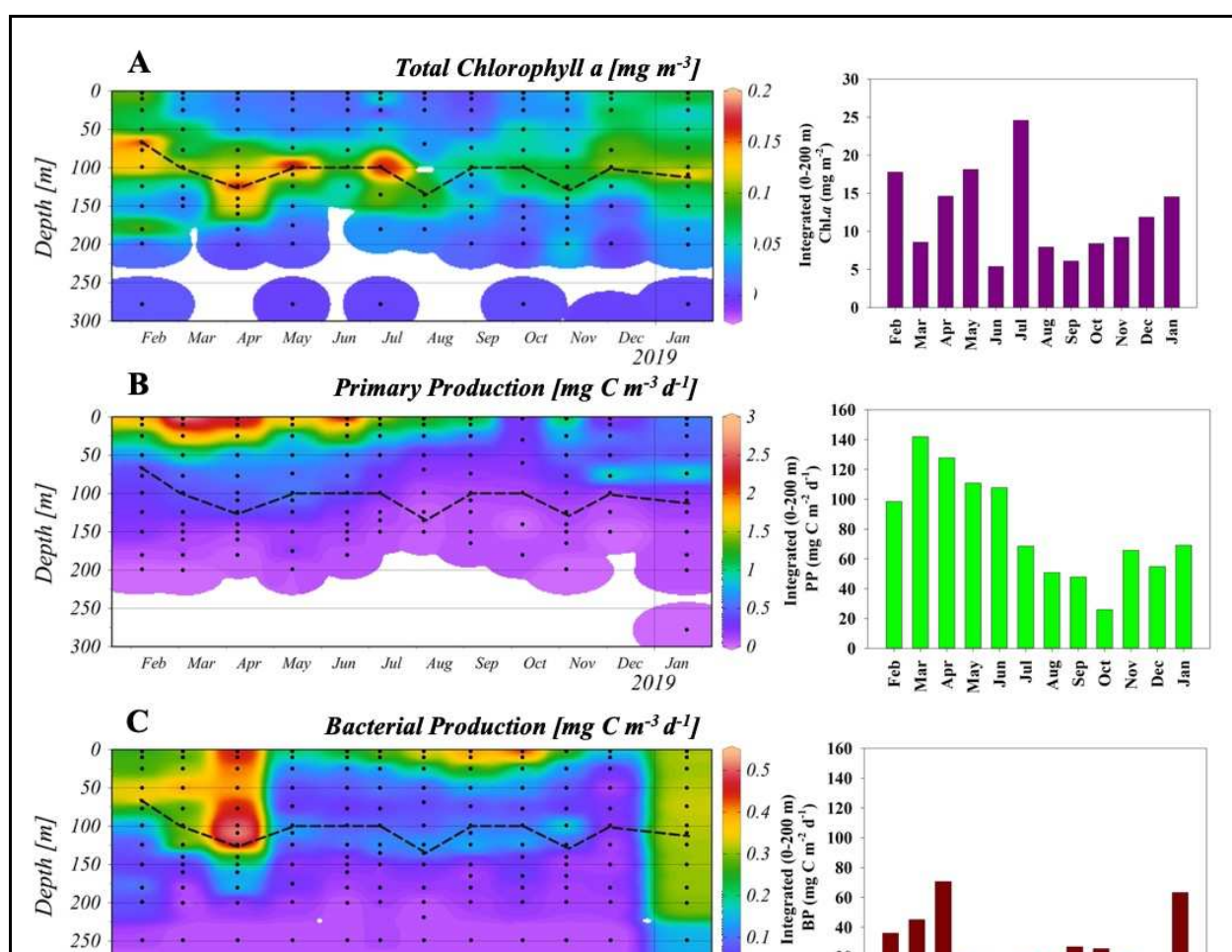


Figure 3: Seasonal changes in depth-resolved (left panels) and depth-integrated (right panels) chlorophyll a (A), primary productivity (B) and bacterial productivity (C). Black dots in panels A-C represent sampling points from each cruise. See Supplementary Figure S4 for the full depth profile of BP to $\sim 1,400$ m.

284

285 Primary productivity (PP) was highest at the surface most of the year ($1-3 \text{ mg C m}^{-3} \text{ d}^{-1}$),
286 declining with depth, with no observable maximum during most of the year at the DCM
287 ($0.08-0.47 \text{ mg C m}^{-3} \text{ d}^{-1}$, Figure 3B). This is consistent with the chlorophyll maximum in
288 ultra-oligotrophic oceans being decoupled from the PP maximum (Lazzari et al., 2012). An
289 exception to this decoupling was observed during December 2019 and January 2020, where a

290 peak of PP was observed at around 75 m ($0.93\text{-}0.96 \text{ mg C m}^{-3} \text{ d}^{-1}$), slightly above the DCM
291 (Figure 3B). The observed values at the surface are within the range or somewhat lower than
292 previously measured values in the EMS (typically around $\sim 2 \text{ mg C m}^{-3} \text{ day}^{-1}$, but with values
293 as high as $\sim 18 \text{ mg C m}^{-3} \text{ day}^{-1}$ recorded), (Hazan et al., 2018; Rahav et al., 2013). The
294 integrated PP values ranged between $69\text{-}142 \text{ mg C m}^{-2} \text{ d}^{-1}$ during the mixing period, and from
295 48 to $113 \text{ mg C m}^{-2} \text{ d}^{-1}$ during the stratified months (Figure 3B). These values are within the
296 ranges observed in other studies of this region (reviewed in (Berman-Frank and Rahav, 2012;
297 Siokou-Frangou et al., 2010) and discussed below). Our measurements result in an annual PP
298 of $\sim 32 \text{ gC m}^{-2}$, which is lower by $\sim 50\%$ than most estimates from the EMS (Boldrin et al.,
299 2002; Psarra et al., 2000). These annual estimates highlight the ultra-oligotrophic
300 characteristics of the easternmost Levantine Basin.

301 During most of the year BP was highest at the surface ($\sim 0.2\text{-}0.5 \text{ mg C m}^{-3} \text{ d}^{-1}$, Figure 3C,
302 Supplementary Figure S4), within the range of previous observations at this area (Rahav et
303 al., 2019; Tanaka et al., 2007; Van Wambeke et al., 2000). However, BP differed from PP in
304 several aspects. First, a significant increase in BP was observed during April, with the highest
305 rate observed at $\sim 110 \text{ m}$ where the DCM was detected. Indeed, a smaller secondary peak in
306 BP was observed at a depth corresponding to the DCM throughout the year (Figure 3C).
307 Second, surface BP increased during summer from a minimum in May to a maximum in
308 September-October, before decreasing again. Third, during January 2019 a large increase was
309 observed in BP, which was more-or-less homogenously distributed throughout the water
310 column down to $\sim 200 \text{ m}$. Depth-integrated BP ranged from a maximum of $\sim 70 \text{ mg C m}^{-2} \text{ d}^{-1}$
311 during April 2018 and January 2019 to a minimum of $\sim 20 \text{ mg C m}^{-2} \text{ d}^{-1}$ during May-
312 December 2018, within the range of previous measurements $\sim 10\text{-}45 \text{ mg C m}^{-2} \text{ day}^{-1}$ (e.g.
313 (Christaki et al., 2011; Robarts et al., 1996; Van Wambeke et al., 2000). The integrated PP to

314 BP ratio also differed between the mixed and stratified periods. Where, during the mixed
315 season the PP:BP ratio was ~3:1, while during the stratified period it reached ~5:1.

316

317 **3.3 Phytoplankton abundance and specific functional groups**

318 Picocyanobacteria (*Prochlorococcus* and *Synechococcus*) were the most abundant
319 picophytoplankton cells throughout the year (Figure 4, Supplementary Figure S5).
320 *Prochlorococcus* was more abundant during the stratified period, and predominated below
321 the mixed layer (Figure 4A). Based on the ratio of divinyl chlorophyll a to total chlorophyll a
322 (Figure 5A), *Prochlorococcus* contributed up to ~45% of the total phytoplankton biomass at
323 the DCM during late fall (Figure 5A). *Synechococcus* was more abundant during the mixed
324 period and in the surface waters (Figure 4B). Pico-eukaryotes were present at up to 10^4 cells
325 ml⁻¹ during February-June (Figure 4C), but there was no clear group-specific signal in the
326 tested photosynthetic pigments during this period (Figure 5B-D), and thus the specific pico-
327 eukaryotic groups present at this time could not be identified. In contrast, the presence of 19-
328 hexanoyloxyfucoxanthin and 19-butanoyloxyfucoxanthin (19-Hex+19-But), primarily during
329 August to November (Figure 5B), suggests the presence of haptophytes, and this was
330 corroborated with microscopic identification of coccolithophores (see a more detailed
331 discussion in Keuter et al, *in prep*). Finally, peridinin and fucoxanthin peaked during January,
332 suggesting the presence of dinoflagellates and diatoms, respectively (Figure 5C,D).

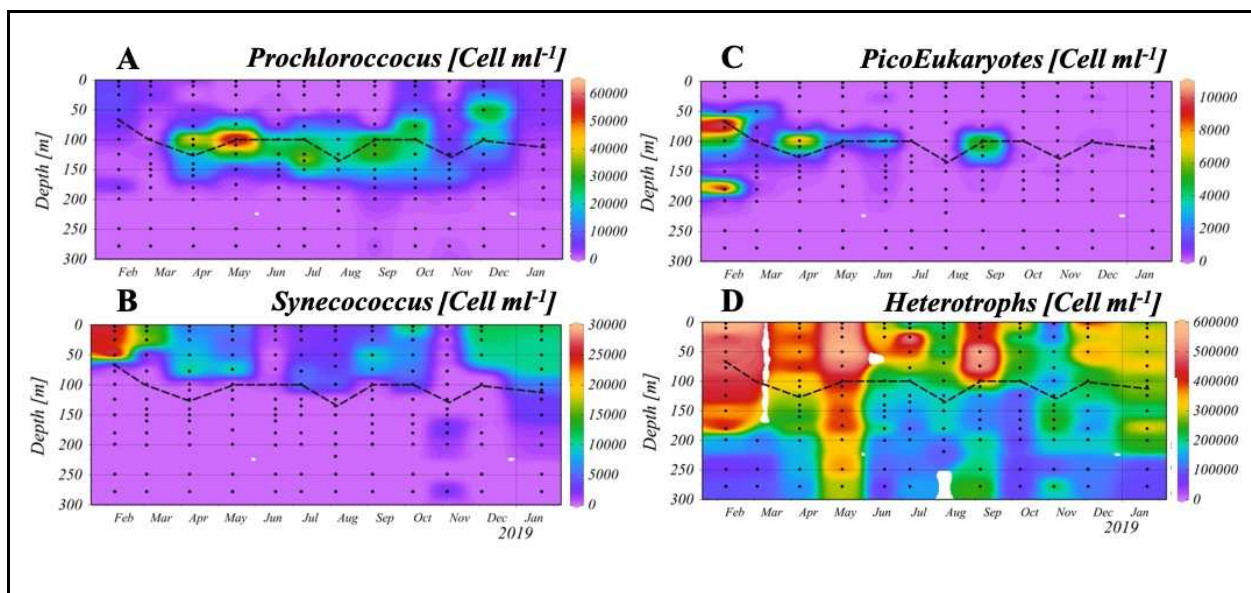


Figure 4: Annual dynamics of monthly measured picophytoplankton and heterotrophic bacterial abundance: *Prochlorococcus* (A), *Synechococcus* (B), PicoEukaryotes (C) and heterotrophic bacteria (D) at the THEMO2 station. Black dots represent sample point from each cruise. No data were available from the March cruise for total microbial counts. Note the differences in the color scale for each plot. Dashed line represents the DCM. See Supplementary Figure S5 for the full depth profiles to ~1,400m.

333

334 Throughout the year, total prokaryotic microbial counts (Sybr-stained cells, thus including
335 cyanobacteria, heterotrophic bacteria and archaea) ranged between 3×10^5 to 6×10^5 cells ml⁻¹,
336 with higher values observed during February and May (Figure 3SB). Heterotrophic bacteria
337 were much more abundant than the combined phototrophs, the latter forming 2.4-8.5% of the
338 total Sybr-stained cell counts (Figure 4D). Below the photic layer, cell counts were typically
339 lower, ranging from 1.9×10^4 - 4.5×10^5 cells ml⁻¹ (Supplementary Figure S5).

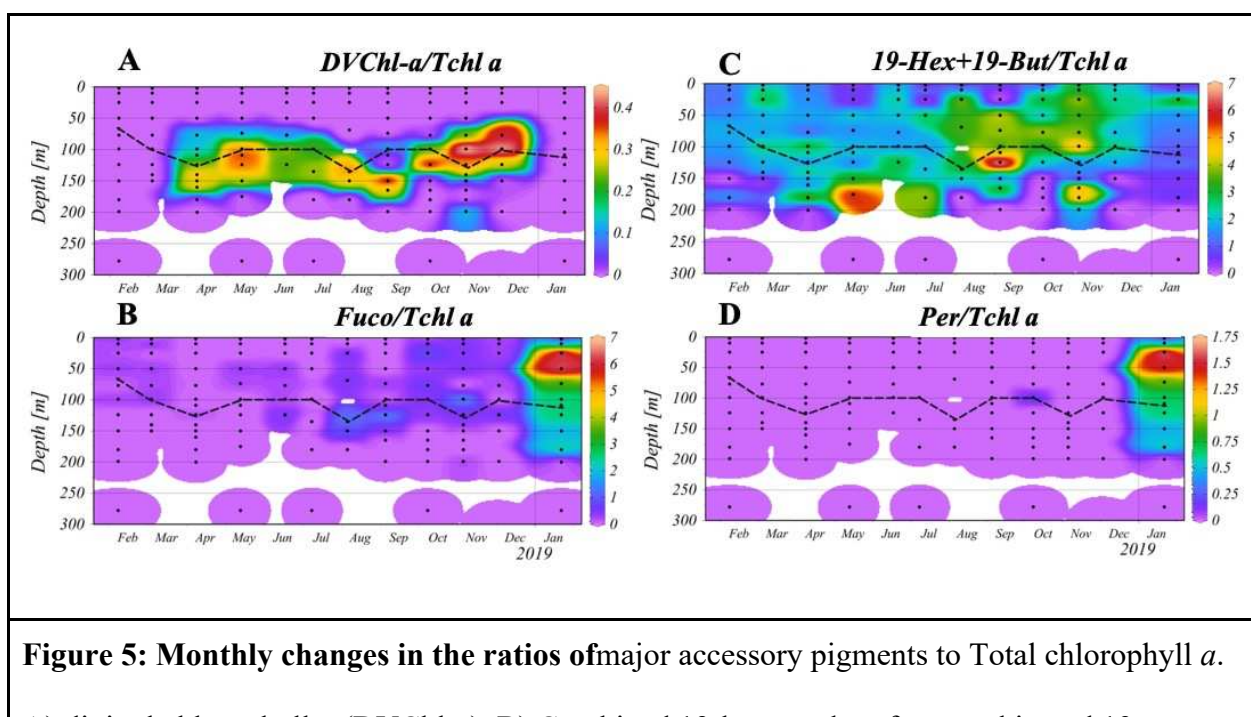


Figure 5: Monthly changes in the ratios of major accessory pigments to Total chlorophyll *a*.

A) divinyl chlorophyll *a* (DVChl-*a*). B) Combined 19-hexanoyloxyfucoxanthin and 19-butanoyloxyfucoxanthin (19-Hex+19-But). C) Fucoxanthin (Fuco). D) Peridinin. Black dots represent sampling depths. Dashed line represents the DCM.

340

341 **4 Discussion**

342 **4.1 How oligotrophic is the EMS compared to other oligotrophic oceans?**

343 The EMS has previously been suggested to be one of the most oligotrophic marine systems
344 on Earth, including a claim for the “deepest Secchi-depth world record” - 53 m during
345 summertime (Berman et al., 1984). A comparison of published values of PP, including those
346 measured in this study, supports this notion, with the median integrated PP being ~66% lower
347 than Bermuda, the Red Sea and the Western Mediterranean Sea (WMS), and ~80% lower
348 than station ALOHA (HOT) (Figure 6A). Our estimates of PP during the SoMMoS cruises
349 are among the lowest in the EMS (Figure 6A), yielding an annual PP of ~32-39 gC m⁻² y⁻¹,
350 although similar values have previously been reported (Dugdale and Wilkerson, 1988). The
351 annual PP during the SoMMoS cruises is approximately half of that reported above the
352 continental slope of the Cretan Sea, ~59 gC m⁻² y⁻¹, (Psarra et al., 2000), as well as in other

353 more western locations in the EMS, $\sim 62 \text{ gC m}^{-2} \text{ y}^{-1}$ (Boldrin et al., 2002). It should be noted,
354 though, that our incubation approach do not precisely mimic the *in-situ* illumination and
355 temperature at the time of sampling, which, based on our previous work, may underestimate
356 the actual PP rates by up to $\sim 20\%$ (Figure S2). Under these circumstances, the annual PP we
357 report may reach $\sim 39 \text{ gC m}^{-2} \text{ y}^{-1}$, approximately $\sim 33\%$ lower than previously reported from
358 the EMS (Psarra et al., 2000; Boldrin et al., 2002). Moreover, comparison between different
359 studies that used similar, yet not identical, methodology for PP estimates, should be done
360 with care. For example, in the comparison presented in Figure 6A many of the studies
361 measured PP from dawn to dusk while in this study we used longer incubations which
362 account for the whole day (net PP). These differences may also, partly, account for the
363 changes between the different oceanic locations, yet even with these caveats taken into
364 account the PP in the EMS is still lower than other oceanic regions (Figure 6A).
365 The values of integrated chlorophyll (Table 1, Figure 2A) and phytoplankton cell counts are
366 also somewhat lower than previously-published measurements from the same region (Figure
367 4, Figure 7) (Berman et al., 1984; Robarts et al., 1996). Both the temperature and salinity
368 minima during the SoMMoS cruise series were higher than the 2002-2020 climatological
369 average (Herut et al., 2020), and thus we currently cannot determine whether the lower PP
370 values measured during this annual cruise series are due to inter-annual variability, or
371 whether these are due to the possible underestimation of the PP values discussed above
372 (section 2.2). Nevertheless, it is clear that the EMS is one of the most oligotrophic locations
373 on Earth, as defined using primary production, and that key seasonal dynamics are similar
374 between studies performed a decade apart (compare Figures 7D, E).
375 In addition to low PP, the EMS exhibits low sinking fluxes of particulate organic carbon
376 (POC). The POC flux measured from the bottom of the photic layer (180 m) at the DeepLev
377 mooring station, which is in the same region as the THEMO-2 site (Figure 1A, $\sim 10\text{Km}$ north

378 of our study site, Lat: 32.820 N; 34.380 E), is $\sim 0.2 \text{ gC m}^{-2}$ during the summer months (May-
379 September 2018) and $\sim 0.8 \text{ gC m}^{-2}$ per year (Alkalay et al., 2020). This POC flux to the
380 aphotic layer is less than 2% of the PP measured during summertime ($\sim 12 \text{ gC m}^{-2}$ in 5
381 months) or 2.5% from the annual PP rates ($\sim 32 \text{ gC m}^{-2} \text{ y}^{-1}$). The fraction of PP exported as
382 particulate matter in the EMS is therefore lower than that reported in other oligotrophic
383 systems; i.e., HOT and BATS stations $\sim 5\%$ (Karl and Church, 2014; Steinberg et al., 2001).
384 This low contribution provides an additional biogeochemical implication of the extreme
385 oligotrophic conditions of the EMS. It also points to that the dissolved organic carbon
386 fraction derived from PP is rapidly recycled in the photic layer by heterotrophic/mixotrophic
387 bacteria as often observed in LNLC environments, as reviewed in (Santinelli, 2015). We
388 note, however, that estimates of export production based on nitrate+nitrate loss from the
389 photic zone, calculated from the same data, are significantly higher ($172 \text{ mmol N m}^{-2} \text{ year}^{-1}$,
390 corresponding to $\sim 13.6 \text{ g C m}^{-2} \text{ year}^{-1}$, presented in a companion paper, Ben Ezra et al.,
391 2021). The reason for this discrepancy is unclear, but may be due to over-estimation of the
392 export production rates (e.g. if part of the nitrate+nitrite was taken up by heterotrophic
393 organisms) and/or underestimation of the sinking carbon flux from sediment traps, and/or
394 non-Redfield C:N conversion factors that may prevail in the EMS. Moreover, such an
395 underestimation may be due to sinking flux from organisms too large to be caught in the
396 sediment traps such as fish or jellyfish (Edelist et al., 2020).
397 In contrast to PP, integrated BP in the EMS was higher than estimates at BATS and HOT,
398 and similar to the Red Sea (Figure 6B, which compares only measurements obtained using
399 the ^3H -leucine incorporation method). Yet, values obtained in the South Pacific Gyre, 43-61
400 $\text{mg C m}^{-2} \text{ d}^{-1}$, (Berman-Frank et al., 2016) do come close to our measurements in the EMS.
401 Thus, differences in PP between oligotrophic regions are not necessarily coupled to BP
402 measurements. Previous studies, including from HOT and BATS, have shown that BP and PP

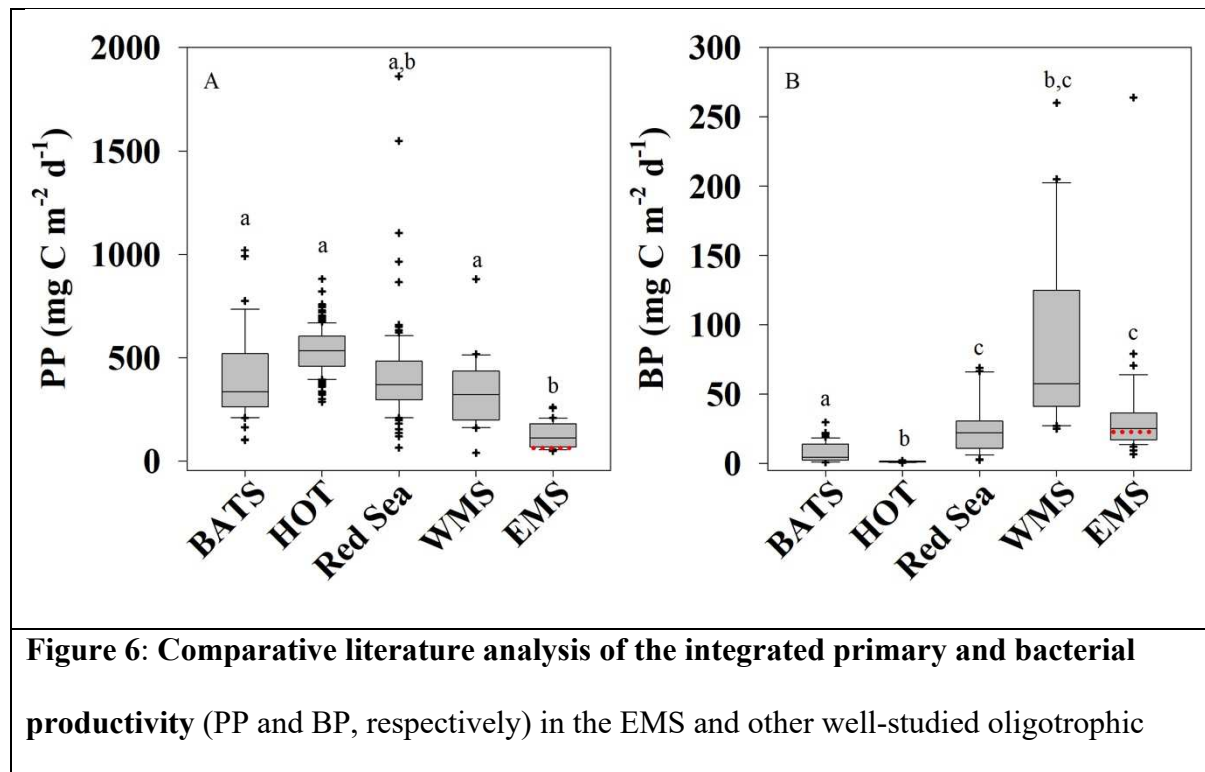
403 are decoupled across multiple time-scales (e.g hours-months) (Viviani and Church, 2017).
404 Similarly, PP and BP were uncoupled in the cyclonic Rhodes Gyre and the anti-cyclonic
405 Cyprus Eddy of the EMS (Rahav et al., 2013) and also in our study when BP increased in
406 surface waters between June and November, while PP rates declined (Figure 3). One
407 potential reason for this discrepancy is that PP is often measured on filtered samples
408 (particulate PP), and thus does not include the fraction of dissolved organic carbon (DOC)
409 fixed through PP that is released from the cells due to exudation or lysis (Viviani et al.,
410 2015).

411 When phytoplankton have sufficient carbon and light for photosynthesis yet nutrients such as
412 P and N are limiting, photosynthesis is uncoupled from growth and high concentrations of
413 DOC are often released to the environment (Berman-Frank and Dubinsky, 1999). Previous
414 studies from natural samples and from cultures of the numerically-dominant phytoplankton in
415 the EMS, *Prochlorococcus* and *Synechococcus*, suggest a potentially high but variable
416 fraction of released DOC (typically 20-70% of PP, with one study suggesting >90% in lab
417 cultures, (Roth-Rosenberg et al., 2020; Viviani et al., 2015). It is currently unclear whether
418 autochthonous production (that is, local PP) is sufficient to support the growth requirements
419 of heterotrophic bacteria, given what is known about the growth efficiency of bacteria. A
420 study from the Cretan Sea suggesting that this is possible if the release of DOC from
421 phytoplankton exceeds 40% of PP (Anderson and Turley, 2003).

422 The EMS is affected by coastal intrusions of relatively chlorophyll-rich waters (Efrati et al.,
423 2013), which could contribute also additional DOC, yet the importance of these processes in
424 determining BP and PP requires additional studies, as they occur on temporal and spatial
425 scales not captured by the SoMMoS cruise series. Such studies are also needed to understand
426 the relative contribution of dissolved compared to particulate carbon to export processes in
427 oligotrophic regions.

428 An additional explanation for the uncoupling between PP and BP was previously suggested
429 following an *in-situ* phosphorus addition experiment at an anti-cyclonic eddy in the EMS,
430 where orthophosphate addition led to chlorophyll *a* decrease while heterotrophic biomass and
431 activity increased (Thingstad et al., 2005). The authors postulated two possible scenarios to
432 explain their observation; 1) fast growing bacteria out-competed phytoplankton for the added
433 phosphorus. Then, the accumulated heterotrophic biomass was quickly channeled toward
434 larger consumers (the ‘bypass hypothesis’). 2) luxury uptake of P, mainly by heterotrophic
435 bacteria (and to a lesser extent by small-size picophytoplankton), formed a phosphorus-rich
436 diet for grazers, resulting in increased egg production (the ‘tunneling hypothesis’).
437 Additionally, a scenario where an increase in temperature drives increased growth by
438 heterotrophic bacteria (Luna et al., 2012), resulting in a draw-down of inorganic nutrients,
439 could explain the increased BP in surface waters during summer, when no increase in PP was
440 observed (Figure 3).

441



locations (Bianchi et al., 1999; Bonnet et al., 2011; Casotti et al., 2003; Christaki et al., 2011; Decembrini et al., 2009; Fernández et al., 1994; Gasol et al., 1998; Gaudy et al., 2003; Hazan et al., 2018; Ignatiades et al., 2002; Lemée et al., 2002; Lohrenz et al., 1988; Morán and Estrada, 2001; Moutin and Raimbault, 2002; Pedrós-Alió et al., 1999; Rahav et al., 2019; Eyal Rahav et al., 2013; Robarts et al., 1996; Siokou-Frangou et al., 2002; Van Wambeke et al., 2004; Vidussi et al., 2000; Wambeke et al., 2002; Zervoudaki et al., 2007). Box-Whisker plots show the interquartile range (25th–75th percentile) of the data set. The horizontal line within the box represents the median value. The red dashed line in the EMS boxes shows the median values for the SoMMoS cruises described here. The letters above the box-plots represent significant differences (ANOVA, $p < 0.05$) for mean values between sampling sites. The BP compilation includes only measurements obtained using the ^3H -leucine incorporation method. Note the different Y axis.

442

443 **4.2 Who are the main phytoplankton in the EMS?**

444 During the thermally mixed period, *Synechococcus* were more abundant than
445 *Prochlorococcus* at the upper ~100 m (Figures 4). This period was characterized by
446 measurable N at the surface while P concentrations were still extremely low – possibly
447 causing P limitation (December-July, Table 1, Ben Ezra et al., 2021). In contrast, the
448 extreme surface nutrient scarcity during the stratified period, when both N and P were below
449 the limit of detection and were potentially co-limiting (Ben Ezra et al., 2021), likely
450 contributed to the dominance of the small-size cyanobacterium *Prochlorococcus* over the
451 somewhat larger-cell *Synechococcus* (Figures 4). It is generally accepted that, as the nutrient
452 concentrations decrease (i.e., the water becomes more oligotrophic), so does the average size
453 of phytoplankton (Margalef and Kinne, 1997). Additionally, while most *Synechococcus*
454 genomes encode the genes required for nitrate uptake and utilization, this trait is found only

455 in a subset of the *Prochlorococcus* genomes (Berube et al., 2018), and single-cell analysis
456 suggests that more *Synechococcus* cells in nature utilize nitrate compared to *Prochlorococcus*
457 (Berthelot et al., 2019). Thus, the type of nutrient limitation, P or N+P, (Krom et al., 1991;
458 Thingstad et al., 2005; Zohary et al., 2005) may also affect the temporal dynamics of these
459 two clades in the water column.

460 The abundances of these two cyanobacterial groups also differed with depth. *Synechococcus*
461 was more abundant in the surface waters than *Prochlorococcus* (Fig 4). This was especially
462 evident from May to September when *Prochlorococcus* cells could not be identified in the
463 surface layer using either flow cytometry or pigment analysis (Figures 4 and 5). While the
464 low *Prochlorococcus* abundance at the surface could be partly due to the limit of detection of
465 the flow cytometer used, it is supported by the lack of observed DVChl-a (Figure 5a) and by
466 previous genetic analyses (Rosenberg et al., 2020). It has been suggested that
467 *Prochlorococcus*' unique photosynthetic pigments (DVChl-a and DVChl-b) provide a
468 competitive advantage for these organisms at deeper layers of the water column, leading to a
469 niche separation between these two pico-cyanobacteria (Moore et al., 1995). The observed
470 niche (depth) separation between *Prochlorococcus* and *Synechococcus* has been previously
471 observed including in the first description of *Prochlorococcus* from the North Atlantic and
472 North Pacific (Chisholm et al., 1988), and the Eastern South Pacific (BIOSOPE cruise,
473 (Huang et al., 2015)). However, this is not a universal observation. At the HOT station in the
474 North Pacific, *Prochlorococcus* and *Synechococcus* often show similar depth distributions,
475 both being more abundant at the surface, with *Prochlorococcus* more abundant numerically
476 and in terms of biomass (van den Engh et al., 2017). Similarly, in the Indian Ocean during
477 May-June 2003 *Prochlorococcus* dominated the surface waters whereas *Synechococcus* were
478 much less abundant (Huang et al., 2015). Indeed, a global analysis of >35,000 quantitative
479 measurements of *Prochlorococcus* and *Synechococcus* found that *Prochlorococcus* were

480 often more abundant than *Synechococcus* at high PAR and temperature values representative
481 of surface waters in tropical waters (Flombaum et al., 2013). Thus, the reasons why
482 *Prochlorococcus* and *Synechococcus* partitioned by both depth and season in the EMS, and
483 why this is not necessarily observed elsewhere, remain unclear. Other factors probably also
484 impact distribution, as was suggested for surface populations of *Prochlorococcus* that
485 appeared to be negatively affected by atmospheric deposition through biological (e.g.,
486 airborne viruses or other biological agents that infect the cells) and chemical (e.g., trace-
487 metals toxicity) processes (Rahav et al., 2020).

488 While the pico-cyanobacteria *Prochlorococcus* and *Synechococcus* were the most
489 numerically abundant phytoplankton at THEMO-2, when biomass is examined the
490 contribution of picoeukaryotes can be as high as that of the two pico-cyanobacteria, or even
491 higher (Supplementary Figure S6, and see below). A previous study of the diversity of pico-
492 phytoplankton in the EMS showed that pico-eukaryotes were not very common in terms of
493 their DNA sequences or flow cytometry signals, but were often dominant in terms of RNA
494 sequences, one potential proxy for photosynthetic activity (Man-Aharonovich et al., 2010). In
495 that study, pico-eukaryotes were suggested to comprise up to 60% of the photosynthetic
496 picoplankton biomass in surface waters, and were mainly composed of Haptophytes
497 (primarily *Prymnesiophytes*) and *Stramenopiles* (Man-Aharonovich et al., 2010). In
498 agreement with these observations, the photosynthetic pigment 19'-hexanoyloxyfucoxanthin
499 (19'-hex), which is considered (together with 19'-butanoyloxyfucoxanthin, or 19'-but) to be a
500 diagnostic pigment for *prymnesiophytes*, was found year-round in the water column, but was
501 more abundant relative to the total phytoplankton biomass (i.e. in relation to total
502 chlorophyll) during August-October (stratified period). Thus, both molecular evidence (Man-
503 Aharonovich et al., 2010) and biochemical evidence (pigment analysis) point to the
504 importance of prymnesiophytes in the EMS. A companion study from the SoMMoS cruises

505 provides an overview of seasonal dynamic and impact of calcified haptophytes
506 (coccolithophores) during this yearly survey (Keuter et al, *in prep*).
507 Interestingly, we often observed 19'-hex around or below the DCM, including at depths
508 where light intensities are very low and photosynthesis may not provide enough carbon or
509 energy to support growth (Fig 5). Recent studies have unveiled that haptophytes, including
510 coccolithophores, are mixotrophic - capable of acquiring prey by phagotrophy or organic
511 compounds by osmotrophy in addition to photosynthesis (e.g. (Avrahami and Frada, 2020;
512 Godrijan et al., 2020; Tillmann, 1998). Indeed, haptophytes can contribute to large fractions
513 of total bacteriovory in marine settings (Frias-Lopez et al., 2009; Unrein et al., 2014). Further
514 analysis of the DNA samples collected on the SoMMoS cruises may help identify
515 mixotrophy within the phytoplankton clades found at the base of the photic layer (e.g.
516 (Yelton et al., 2016) and help illuminate the metabolic capacities required to support
517 phytoplankton growth in this environment.
518 Pigments associated with diatoms and dinoflagellates, which are often dominant
519 phytoplankton groups (Andersen et al., 1996), were observed at relatively high concentrations
520 only during January 2019 (Figure 5C, D). At this time DVChl-*a* measurement were below the
521 detection limit in the water column, suggesting a succession from pico-cyanobacteria to
522 larger eukaryotic organisms, which occurred relatively rapidly - over several weeks. This
523 occurred concomitantly with a drop in surface temperature (Figure 2A) and thus a break in
524 stratification, an increase in nitrate+nitrite (Ben Ezra et al., 2021), and a shift in
525 coccolithophore population towards r-selected species such as *Emiliania huxleyi* which are
526 indicative for a higher nutrient regime (Keuter et al, *in prep*). While chlorophyll-*a*
527 concentrations increased both at the surface (including by satellite sensing, Figure 1B) and at
528 the DCM (Figure 3A), no concomitant increase was measured in PP (Figure 3B). Yet, a
529 major increase was observed in BP (Figure 3C). As described in detail in the materials and

530 methods, our measurements of PP likely underestimate productivity at depth, and the
531 pigments were observed primarily below the mixed layer. It is possible that the
532 phytoplankton bloom actually occurred several days before our cruise, and that the pigments
533 observed are from stressed or dead phytoplankton. In this case, the major increase in BP
534 observed at the time may represent heterotrophic bacteria utilizing dissolved and particulate
535 organic carbon produced during the bloom.

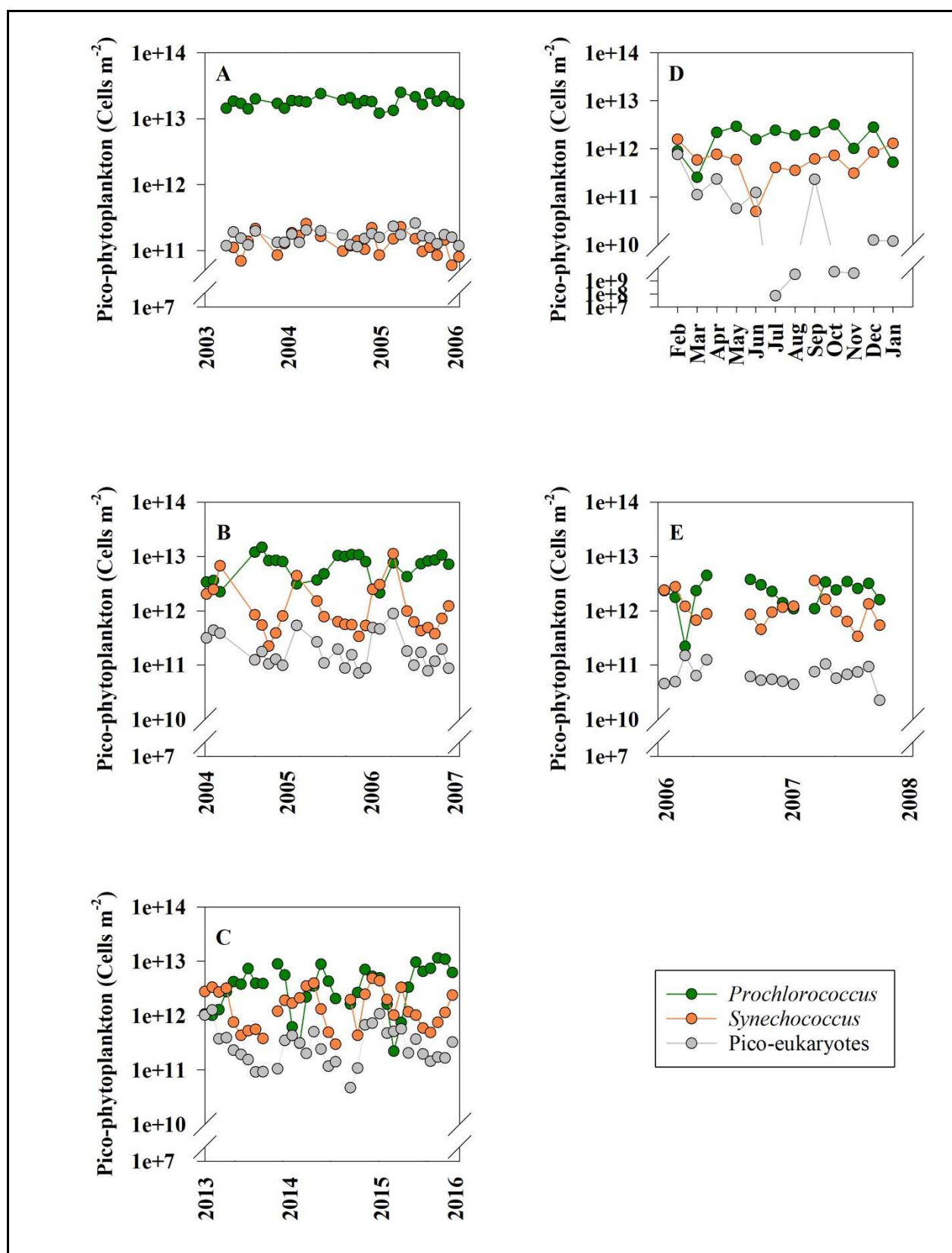


Figure 7: Integrated cell count time series of *Prochlorococcus* (green), *Synechococcus* (orange) and picoeukaryotes (gray) at stations HOT (A), BATS (B), the Northern Red Sea (C), and the EMS (D, E – this study and (Yogeved et al., 2011) respectively). Abundance measurements were carried out using flow cytometry and are presented in a log scale. Data for stations HOT and BATS were compiled from (Malmstrom et al., 2010) and from the Northern Red Sea from the Eilat National Monitoring Program (Shaked and Genin, 2017).

536

537 **4.3 Phytoplankton composition and seasonality in the EMS in comparison to HOT,**
538 **BATS and the Red Sea**

539 The north Atlantic and Pacific gyres, the northern Red Sea and the EMS are all considered
540 Low-Nutrient Low-Chlorophyll marine systems, with phytoplankton numerically dominated
541 by pico-cyanobacteria throughout most of the year. Nevertheless, there are differences in the
542 compositions and the seasonal dynamics of the different phytoplankton clades among these
543 LNLC location (Fig. 7, Sup Fig. 5). Specifically, BATS, the Red Sea and the EMS all show
544 seasonal succession patterns in the abundance of the main phytoplankton groups, although
545 there are subtle differences between these sites: i) The period when integrated *Synechococcus*
546 numbers are higher than *Prochlorococcus* is consistently longer in the Red Sea and EMS (3-4
547 months) compared to BATS (1-2 months); ii) *Prochlorococcus* reached higher absolute cell
548 abundances during the stratified period at BATS ($\sim 10^{13}$ cells m^{-2}) compared to the Northern
549 Red Sea or the EMS ($\sim 2.5 \times 10^{11}$ cells m^{-2}); iii) In terms of calculated biomass, the Red Sea is
550 dominated by pico-eukaryotes for much of the year, whereas in BATS and the EMS the
551 contribution of *Prochlorococcus*, *Synechococcus* and pico-eukaryotes to the total biomass is
552 similar, and the dominant groups change over the year (Supporting Fig S6).
553 The absolute nutrient concentrations and the identity of the limiting nutrient(s) are different
554 between these locations. For example, BATS is typically considered P limited, whereas the

555 EMS is potentially P limited during winter and co-limited by N and P during summer
556 (Zohary et al., 2005). There may also be differences in the length of the mixed period, its
557 intensity, or the composition of the mixed water (e.g. deep water in the EMS have an N:P
558 ratio of ~28:1, compared to the canonical 16:1 Redfield ratio (Redfield, 1934). Future work
559 may use the observed differences in phytoplankton dynamics as a sensitive “readout” of the
560 system, enabling a better understanding of the oceanographic processes underlying the
561 differences between BATS, the Red Sea and the EMS.

562 In contrast to BATS, the Red Sea and the EMS, seasonality at HOT is much less
563 pronounced (Figure 7). *Prochlorococcus* are about 2-orders of magnitude more abundant than
564 *Synechococcus* and pico-eukaryotes, and are also the most dominant in terms of biomass (Sup
565 Fig. 5). The drivers of phytoplankton temporal dynamics at HOT are thus likely
566 fundamentally different compared to BATS, the Red Sea and the EMS. It has been suggested
567 that a-periodic events such as mesoscale eddies, Fe deposition from winds, and biological
568 processes such as dinitrogen fixation, may be major drivers of phytoplankton dynamics at
569 HOT (Karl and Church, 2014) and less so in the EMS (Berman-Frank and Rahav, 2012;
570 Yogeved et al., 2011).

571

572 **5 Closing remarks**

573 The year of data presented here show that the EMS is one of the most oligotrophic regions in
574 the global oceans, as estimated based on PP (32 mg C m⁻² year⁻¹), chlorophyll a (median ~10
575 mg m⁻²), and dominance of small-size picophytoplankton with overall low abundances
576 compared to other LNLC regions (in some cases ~2 orders of magnitude lower). In contrast,
577 BP in the EMS is higher than at HOT and BATS, and similar to the Red and Western
578 Mediterranean seas. This suggests that the system is overall heterotrophic, and that different
579 factors might limit phytoplankton and heterotrophic bacteria (e.g. (Thingstad et al., 2005).

580 Despite these observations, there is a clear seasonal cycle in the phytoplankton populations
581 and their activities, reminiscent of BATS and the Northern Red Sea (but not of HOT),
582 suggesting that mixing (and potentially other seasonal processes such as dust deposition)
583 drive similar processes across many, but not all, LNLC regions.

584 Our results also highlight important knowledge gaps regarding the EMS. For example, we do
585 not know to what extent the bacterial populations or their physiological traits (e.g. bacterial
586 carbon demand or growth efficiency) differ seasonally or vertically in the EMS, as well as
587 compared to other LNLC locations. Detailed studies are also lacking of higher trophic levels
588 in this region (dominant micro-grazer species, diversity, biomass, grazing rates, etc.). These
589 are critical for understanding ecosystem dynamics including top-down vs. bottom-up
590 regulations etc. Biogeochemical characterization of the EMS will also benefit from more
591 explicit characterization of carbon-per-cell estimates, used to derive the biomass
592 contributions from flow-cytometry counts (i.e. Supplementary Figure S6) can vary depending
593 on taxonomy and physiological state (Kirchman, 2013). Future studies of these aspects,
594 together with other data emerging from the SoMMoS cruise series and the ocean
595 observatories in the EMS, should provide the needed background for governments and other
596 stakeholders to employ science-based environmental policies in this rapidly changing region.

597 **Acknowledgements**

598 We thank the captains and crew of the R/V Mediterranean Explorer (EcoOcean) and R/V
599 Bat-Galim (IOLR), Oshra Yosef, Elad Rachmilovitz, Guy Sisma-Ventura for help with the
600 sampling. The SoMMoS ship-time was funded by the Leon H. Charney School of Marine
601 Sciences with help from EcoOcean and IOLR. This study was supported by grant
602 RGP0020/2016 from the Human Frontiers Science Program (to DS), by grant number
603 1635070/2016532 from the NSF-BSF program in Oceanography (NSFOCE-BSF, to DS), and
604 partly by the Israel Science Foundation (grants number 1211/17 to ER and BH and 996/08 to
605 I. B-F and B.H). This study is in partial fulfilment of the M.Sc. thesis of Tom Reich
606 (University of Haifa).

607

608 **Author Contributions**

609 MDK, YL, ER and DS initiated and designed study; TR, TBE, NB, DRR, OB, MDK, ER and
610 DS collected samples; TR, TBE, NB and AT analyzed samples with help from MDK, DA,
611 DRR and SG; TR, ER and DS wrote the manuscript with input from all co-authors.

612 **References**

613

614 Alkalay, R., Zlatkin, O., Katz, T., Herut, B., Halicz, L., Berman-Frank, I., Weinstein, Y.,

615 2020. Carbon export and drivers in the southeastern Levantine Basin. Deep. Res. Part II

616 Top. Stud. Oceanogr. 171, 104713. <https://doi.org/10.1016/j.dsr2.2019.104713>

617 Anabalón, V., Morales, C.E., González, H.E., Menschel, E., Schneider, W., Hormazabal, S.,

618 Valencia, L., Escribano, R., 2016. Micro-phytoplankton community structure in the

619 coastal upwelling zone off Concepción (central Chile): Annual and inter-annual

620 fluctuations in a highly dynamic environment. Prog. Oceanogr. 149, 174–188.

621 <https://doi.org/10.1016/j.pocean.2016.10.011>

622 Andersen, R.A., Bidigare, R.R., Keller, M.D., Latasa, M., 1996. A comparison of HPLC

623 pigment signatures and electron microscopic observations for oligotrophic waters of the

624 North Atlantic and Pacific Oceans. Deep. Res. Part II Top. Stud. Oceanogr. 43, 517–

625 537. [https://doi.org/10.1016/0967-0645\(95\)00095-x](https://doi.org/10.1016/0967-0645(95)00095-x)

626 Anderson, T.R., Turley, C.M., 2003. Low bacterial growth efficiency in the oligotrophic

627 eastern Mediterranean Sea: A modelling analysis. J. Plankton Res. 25, 1011–1019.

628 <https://doi.org/10.1093/plankt/25.9.1011>

629 Avrahami, Y., Frada, M.J., 2020. Detection of Phagotrophy in the Marine Phytoplankton

630 Group of the Coccolithophores (Calcihaptophycidae, Haptophyta) During Nutrient-

631 replete and Phosphate-limited Growth. J. Phycol. 56, 1103–1108.

632 <https://doi.org/10.1111/jpy.12997>

633 Azov, Y., 1986. Seasonal patterns of phytoplankton productivity and abundance in nearshore

634 oligotrophic waters of the Levant Basin (Mediterranean). J. Plankton Res. 8, 41–53.

635 <https://doi.org/10.1093/plankt/8.1.41>

636 Behrenfeld, M.J., 2010. Abandoning sverdrup's critical depth hypothesis on phytoplankton

637 blooms. *Ecology* 91, 977–989. <https://doi.org/10.1890/09-1207.1>

638 Behrenfeld, M.J., Boss, E.S., 2014. Resurrecting the ecological underpinnings of ocean

639 plankton blooms. *Ann. Rev. Mar. Sci.* 6, 167–194. <https://doi.org/10.1146/annurev-marine-052913-021325>

640

641 Berman-Frank, I., Dubinsky, Z., 1999. Balanced Growth in Aquatic Plants: Myth or

642 Reality?<subtitle>Phytoplankton use the imbalance between carbon assimilation and

643 biomass production to their strategic advantage</subtitle>. *Bioscience* 49, 29–37.

644 <https://doi.org/10.1525/bisi.1999.49.1.29>

645 Berman-Frank, I., Rahav, E., 2012. Dinitrogen fixation as a source for new production in the

646 Mediterranean Sea: A review. *Life Mediterr. Sea A Look Habitat Chang.* 199–226.

647 Berman-Frank, I., Spungin, D., Rahav, E., Van Wambeke, F., Turk-Kubo, K., Moutin, T.,

648 2016. Dynamics of transparent exopolymer particles (TEP) during the VAHINE

649 mesocosm experiment in the New Caledonian lagoon. *Biogeosciences* 13, 3793–3805.

650 <https://doi.org/10.5194/bg-13-3793-2016>

651 Berman, T., TOWNSEND, D., EL SAYED, S., TREES, C., AZOV, Y., 1984. Optical

652 transparency, chlorophyll and primary productivity in the eastern Mediterranean near the

653 Israeli coast. *Oceanol. acta* 7, 367–372.

654 Berthelot, H., Duhamel, S., L'Helguen, S., Maguer, J.F., Wang, S., Cetinić, I., Cassar, N.,

655 2019. NanoSIMS single cell analyses reveal the contrasting nitrogen sources for small

656 phytoplankton. *ISME J.* 13, 651–662. <https://doi.org/10.1038/s41396-018-0285-8>

657 Berube, P.M., Rasmussen, A., Braakman, R., Stepanauskas, R., Chisholm, S.W., 2018.

658 Emergence of trait variability through the lens of nitrogen assimilation in

659 *Prochlorococcus*. *bioRxiv*. <https://doi.org/10.1101/383927>

660 Bianchi, F., Boldrin, A., Civitarese, G., Del Negro, P., Giordani, P., Malaguti, A., Socal, G.,

661 Rabitti, S., Turchetto, M.M., 1999. Biogenic particulate matter and primary productivity

662 in the Southern Adriatic and Northern Ionian seas, in: 4th MTP-Workshop MATER. pp.

663 120–121.

664 Boldrin, A., Miserocchi, S., Rabitti, S., Turchetto, M.M., Balboni, V., Socal, G., 2002.

665 Particulate matter in the southern Adriatic and Ionian Sea: Characterisation and

666 downward fluxes. *J. Mar. Syst.* 33–34, 389–410. [https://doi.org/10.1016/S0924-7963\(02\)00068-4](https://doi.org/10.1016/S0924-7963(02)00068-4)

667

668 Bonnet, S., Grosso, O., Moutin, T., 2011. Planktonic dinitrogen fixation along a longitudinal

669 gradient across the Mediterranean Sea during the stratified period (BOUM cruise).

670 *Biogeosciences* 8, 2257–2267. <https://doi.org/10.5194/bg-8-2257-2011>

671 Campbell, L., 2001. Flow cytometric analysis of autotrophic picoplankton. *Methods*

672 *Microbiol.* 30, 317–343.

673 Casotti, R., Landolfi, A., Brunet, C., D'Ortenzio, F., Mangoni, O., Ribera d'Alcalà, M.,

674 Denis, M., 2003. Composition and dynamics of the phytoplankton of the Ionian Sea

675 (eastern Mediterranean). *J. Geophys. Res. Ocean.* 108.

676 <https://doi.org/10.1029/2002jc001541>

677 Chisholm, S.W., Olson, R.J., Zettler, E.R., Goericke, R., Waterbury, J.B., Welschmeyer,

678 N.A., 1988. A novel free-living prochlorophyte abundant in the oceanic euphotic zone.

679 *Nature* 334, 340–343. <https://doi.org/10.1038/334340a0>

680 Christaki, U., Giannakourou, A., Van Wambeke, F., Grégori, G., 2001. Nanoflagellate

681 predation on auto- and heterotrophic picoplankton in the oligotrophic Mediterranean

682 Sea. *J. Plankton Res.* 23, 1297–1310. <https://doi.org/10.1093/plankt/23.11.1297>

683 Christaki, U., Van Wambeke, F., Lefevre, D., Lagaria, A., Prieur, L., Pujo-Pay, M.,

684 Grattepanche, J.D., Colombet, J., Psarra, S., Dolan, J.R., Sime-Ngando, T., Conan, P.,

685 Weinbauer, M.G., Moutin, T., 2011. Microbial food webs and metabolic state across

686 oligotrophic waters of the Mediterranean Sea during summer. *Biogeosciences* 8, 1839–

687 1852. <https://doi.org/10.5194/bg-8-1839-2011>

688 D'Ortenzio, F., Iudicone, D., de Boyer Montegut, C., Testor, P., Antoine, D., Marullo, S.,

689 Santolieri, R., Madec, G., 2005. Seasonal variability of the mixed layer depth in the

690 Mediterranean Sea as derived from in situ profiles. *Geophys. Res. Lett.* 32, 1–4.

691 <https://doi.org/10.1029/2005GL022463>

692 Decembrini, F., Caroppo, C., Azzaro, M., 2009. Size structure and production of

693 phytoplankton community and carbon pathways channelling in the Southern Tyrrhenian

694 Sea (Western Mediterranean). *Deep. Res. Part II Top. Stud. Oceanogr.* 56, 687–699.

695 <https://doi.org/10.1016/j.dsr2.2008.07.022>

696 Diamant, R., Shachar, I., Makovsky, Y., Ferreira, B.M., Cruz, N.A., 2020. Cross-sensor

697 quality assurance for marine observatories. *Remote Sens.* 12, 1–16.

698 <https://doi.org/10.3390/rs12213470>

699 Dugdale, R.C., Wilkerson, F.P., 1988. Nutrient sources and primary production in the Eastern

700 Mediterranean. *Océanographie pélagique méditerranéenne* 179–184.

701 Edelist, D., Guy-Haim, T., Kuplik, Z., Zuckerman, N., Nemoy, P., Angel, D.L., 2020.

702 Phenological shift in swarming patterns of *Rhopilema nomadica* in the Eastern

703 Mediterranean Sea. *J. Plankton Res.* 42, 211–219.

704 <https://doi.org/10.1093/plankt/fbaa008>

705 Efrati, S., Lehahn, Y., Rahav, E., Kress, N., Herut, B., Gertman, I., Goldman, R., Ozer, T.,

706 Lazar, M., Heifetz, E., 2013. Intrusion of coastal waters into the pelagic eastern

707 Mediterranean: In situ and satellite-based characterization. *Biogeosciences* 10, 3349–

708 3357. <https://doi.org/10.5194/bg-10-3349-2013>

709 Fernández, M., Bianchi, M., Van Wambeke, F., 1994. Bacterial biomass, heterotrophic

710 production and utilization of dissolved organic matter photosynthetically produced in the

711 Almeria-Oran front. *J. Mar. Syst.* 5, 313–325. <https://doi.org/10.1016/0924->

712 7963(94)90053-1

713 Flombaum, P., Gallegos, J.L., Gordillo, R.A., Rincón, J., Zabala, L.L., Jiao, N., Karl, D.M.,

714 Li, W.K.W., Lomas, M.W., Veneziano, D., Vera, C.S., Vrugt, J.A., Martiny, A.C., 2013.

715 Present and future global distributions of the marine Cyanobacteria Prochlorococcus and

716 Synechococcus. *Proc. Natl. Acad. Sci. U. S. A.* 110, 9824–9829.

717 <https://doi.org/10.1073/pnas.1307701110>

718 Frias-Lopez, J., Thompson, A., Waldbauer, J., Chisholm, S.W., 2009. Use of stable isotope-

719 labelled cells to identify active grazers of picocyanobacteria in ocean surface waters.

720 *Environ. Microbiol.* 11, 512–525. <https://doi.org/10.1111/j.1462-2920.2008.01793.x>

721 Gasol, J.M., Doval, M.D., Pinhassi, J., Calderón-Paz, J.I., Guixa-Boixareu, N., Vaqué, D.,

722 Pedrós-Alió, C., 1998. Diel variations in bacterial heterotrophic activity and growth in

723 the northwestern Mediterranean Sea. *Mar. Ecol. Prog. Ser.* 164, 107–124.

724 <https://doi.org/10.3354/meps164107>

725 Gaudy, R., Youssara, F., Diaz, F., Raimbault, P., 2003. Biomass, metabolism and nutrition of

726 zooplankton in the Gulf of Lions (NW Mediterranean). *Oceanol. Acta* 26, 357–372.

727 [https://doi.org/10.1016/S0399-1784\(03\)00016-1](https://doi.org/10.1016/S0399-1784(03)00016-1)

728 Genin, A., Zarubin, M., Lindemann, Y., 2018. Deep mixing, stratification and spring

729 phytoplankton bloom in the northern Red Sea, in: 2018 Ocean Sciences Meeting. AGU.

730 Godrijan, J., Drapeau, D., Balch, W.M., 2020. Mixotrophic uptake of organic compounds by

731 cocolithophores. *Limnol. Oceanogr.* 65, 1410–1421. <https://doi.org/10.1002/lno.11396>

732 Guiet, C., Aumont, O., Paytan, A., Bopp, L., Law, C.S., Mahowald, N., Achterberg, E.P.,

733 Marañón, E., Salihoglu, B., Crise, A., Wagener, T., Herut, B., Desboeufs, K.,

734 Kanakidou, M., Olgun, N., Peters, F., Pulido-Villena, E., Tovar-Sanchez, A., Völker, C.,

735 2014. The significance of the episodic nature of atmospheric deposition to Low Nutrient

736 Low Chlorophyll regions. *Global Biogeochem. Cycles* 28, 1179–1198.

737 <https://doi.org/10.1002/2014GB004852>

738 Gunn, K.L., Beal, L.M., Elipot, S., McMonigal, K., Houk, A., 2020. Mixing of subtropical,
739 central, and intermediate waters driven by shifting and pulsing of the agulhas current. *J.*
740 *Phys. Oceanogr.* 50, 3545–3560. <https://doi.org/10.1175/JPO-D-20-0093.1>

741 Hazan, O., Silverman, J., Sisma-Ventura, G., Ozer, T., Gertman, I., Shoham-Frider, E., Kress,
742 N., Rahav, E., 2018. Mesopelagic prokaryotes alter surface phytoplankton production
743 during simulated deep mixing experiments in Eastern Mediterranean Sea waters. *Front.*
744 *Mar. Sci.* 5, 1–11. <https://doi.org/10.3389/fmars.2018.00001>

745 Herut, B., 2015. The National Monitoring Program of Israel's Mediterranean waters –
746 Scientific Report for 2013/14, IOLR Report H21/2015. IOLR.

747 Hooker, S.B., Van Heukelem, L., Thomas, C.S., Claustre, H., Ras, J., Barlow, R., Sessions,
748 H., Schlüter, L., Perl, J., Trees, C., Stuart, V., Head, E., Clementson, L., Fishwick, J.,
749 Llewellyn, C., Aiken, J., 2005. Second SeaWiFS HPLC analysis round-robin experiment
750 (SeaHARRE-2), NASA Technical Memorandum. National Aeronautics and Space
751 Administration, Goddard Space Flight Center.

752 Huang, S., Zhang, S., Jiao, N., Chen, F., 2015. Marine cyanophages demonstrate
753 biogeographic patterns throughout the global ocean. *Appl. Environ. Microbiol.* 81, 441–
754 452. <https://doi.org/10.1128/AEM.02483-14>

755 Ignatiades, L., Psarra, S., Zervakis, V., Pagou, K., Souvermezoglou, E., Assimakopoulou, G.,
756 Gotsis-Skretas, O., 2002. Phytoplankton size-based dynamics in the Aegean Sea
757 (Eastern Mediterranean). *J. Mar. Syst.* 36, 11–28. [https://doi.org/10.1016/S0924-7963\(02\)00132-X](https://doi.org/10.1016/S0924-7963(02)00132-X)

758 Jickells, T.D., 1998. Nutrient biogeochemistry of the coastal zone. *Science* (80-.). 281, 217–
760 222. <https://doi.org/10.1126/science.281.5374.217>

761 Karl, D.M., Church, M.J., 2014. Microbial oceanography and the Hawaii Ocean Time-series

762 programme. *Nat. Rev. Microbiol.* 12, 699–713. <https://doi.org/10.1038/nrmicro3333>

763 Katz, T., Weinstein, Y., Alkalay, R., Biton, E., Toledo, Y., Lazar, A., Zlatkin, O., Soffer, R.,

764 Rahav, E., Sisma-Ventura, G., Bar, T., Ozer, T., Gildor, H., Almogi-Labin, A., Kanari,

765 M., Berman-Frank, I., Herut, B., 2020. The first deep-sea mooring station in the eastern

766 Levantine basin (DeepLev), outline and insights into regional sedimentological

767 processes. *Deep. Res. Part II Top. Stud. Oceanogr.* 171, 104663.

768 <https://doi.org/10.1016/j.dsr2.2019.104663>

769 Kimor, B., Wood, E.J.F., 1975. A plankton study in the eastern Mediterranean Sea. *Mar.*

770 *Biol.* 29, 321–333. <https://doi.org/10.1007/BF00388852>

771 Kirchman, D.L., 2013. Degradation of organic material. *Process. Microb. Ecol.* 79–98.

772 <https://doi.org/10.1093/acprof:oso/9780199586936.003.0005>

773 Krom, M., Kress, N., Berman-Frank, I., Rahav, E., 2014. Past, present and future patterns in

774 the nutrient chemistry of the eastern mediterranean, in: *The Mediterranean Sea: Its*

775 *History and Present Challenges*. Springer, pp. 49–68. https://doi.org/10.1007/978-94-007-6704-1_4

777 Krom, M.D., Kress, N., Brenner, S., Gordon, L.I., 1991. Phosphorus limitation of primary

778 productivity in the eastern Mediterranean Sea. *Limnol. Oceanogr.* 36, 424–432.

779 <https://doi.org/10.4319/lo.1991.36.3.0424>

780 Lazzari, P., Solidoro, C., Ibello, V., Salon, S., Teruzzi, A., Béranger, K., Colella, S., Crise,

781 A., 2012. Seasonal and inter-annual variability of plankton chlorophyll and primary

782 production in the Mediterranean Sea: A modelling approach. *Biogeosciences* 9, 217–

783 233. <https://doi.org/10.5194/bg-9-217-2012>

784 Lemée, R., Rochelle-Newall, E., Van Wambeke, F., Pizay, M.-D., Rinaldi, P., Gattuso, J.-P.,

785 2002. Seasonal variation of bacterial production, respiration and growth efficiency in the

786 open NW Mediterranean Sea. *Aquat. Microb. Ecol.* 29, 227–237.

787 Letelier, R.M., Dore, J.E., Winn, C.D., Karl, D.M., 1996. Seasonal and interannual variations
788 in photosynthetic carbon assimilation at station ALOHA. Deep. Res. Part II Top. Stud.
789 Oceanogr. 43, 467–490. [https://doi.org/10.1016/0967-0645\(96\)00006-9](https://doi.org/10.1016/0967-0645(96)00006-9)

790 Lohrenz, S.E., Wiesenburg, D.A., DePalma, I.P., Johnson, K.S., Gustafson Jr, D.E., 1988.
791 Interrelationships among primary production, chlorophyll, and environmental conditions
792 in frontal regions of the western Mediterranean Sea. Deep Sea Res. Part A. Oceanogr.
793 Res. Pap. 35, 793–810.

794 Luna, G.M., Bianchelli, S., Decembrini, F., De Domenico, E., Danovaro, R., Dell'Anno, A.,
795 2012. The dark portion of the Mediterranean Sea is a bioreactor of organic matter
796 cycling. Global Biogeochem. Cycles 26.

797 Malmstrom, R.R., Coe, A., Kettler, G.C., Martiny, A.C., Frias-Lopez, J., Zinser, E.R.,
798 Chisholm, S.W., 2010. Temporal dynamics of Prochlorococcus ecotypes in the Atlantic
799 and pacific oceans. ISME J. 4, 1252–1264. <https://doi.org/10.1038/ismej.2010.60>

800 Man-Aharonovich, D., Philosof, A., Kirkup, B.C., Le Gall, F., Yoge, T., Berman-Frank, I.,
801 Polz, M.F., Vaulot, D., Béjà, O., 2010. Diversity of active marine picoeukaryotes in the
802 Eastern Mediterranean Sea unveiled using photosystem-II psbA transcripts. ISME J. 4,
803 1044–1052. <https://doi.org/10.1038/ismej.2010.25>

804 Margalef, R., Kinne, O., 1997. Excellence in Ecology. Germany: Ecology Institute.

805 Marty, J.-C.C., Chiavérini, J., Pizay, M.-D.D., Avril, B., 2002. Seasonal and interannual
806 dynamics of nutrients and phytoplankton pigments in the western Mediterranean Sea at
807 the DYFAMED time-series station (1991–1999). Deep Sea Res. Part II Top. Stud.
808 Oceanogr. 49, 1965–1985. [https://doi.org/10.1016/S0967-0645\(02\)00022-X](https://doi.org/10.1016/S0967-0645(02)00022-X)

809 Marty, J.C., Chiavérini, J., 2010. Hydrological changes in the Ligurian Sea (NW
810 Mediterranean, DYFAMED site) during 1995–2007 and biogeochemical consequences.
811 Biogeosciences 7.

812 Mena, C., Reglero, P., Hidalgo, M., Sintes, E., Santiago, R., Martín, M., Moyà, G., Balbín,
813 R., 2019. Phytoplankton community structure is driven by stratification in the
814 oligotrophic mediterranean sea. *Front. Microbiol.* 10.
815 <https://doi.org/10.3389/fmicb.2019.01698>

816 Moore, L.R., Goericke, R., Chisholm, S.W., 1995. Comparative physiology of
817 *Synechococcus* and *Prochlorococcus*: influence of light and temperature on growth,
818 pigments, fluorescence and absorptive properties. *Mar. Ecol. Prog. Ser.* 259–275.

819 Morán, X.A.G., Estrada, M., 2001. Short-term variability of photosynthetic parameters and
820 particulate and dissolved primary production in the Alboran Sea (SW Mediterranean).
821 *Mar. Ecol. Prog. Ser.* 212, 53–67.

822 Moutin, T., Raimbault, P., 2002. Primary production, carbon export and nutrients availability
823 in western and eastern Mediterranean Sea in early summer 1996 (MINOS cruise). *J.*
824 *Mar. Syst.* 33, 273–288.

825 Nielsen, E.S., 1952. The use of radio-active carbon (c14) for measuring organic production in
826 the sea. *ICES J. Mar. Sci.* 18, 117–140. <https://doi.org/10.1093/icesjms/18.2.117>

827 Ozer, T., Gertman, I., Kress, N., Silverman, J., Herut, B., 2017. Interannual thermohaline
828 (1979–2014) and nutrient (2002–2014) dynamics in the Levantine surface and
829 intermediate water masses, SE Mediterranean Sea. *Glob. Planet. Change* 151, 60–67.
830 <https://doi.org/10.1016/j.gloplacha.2016.04.001>

831 Pedrós-Alió, C., Calderón-Paz, J.-I., Guixa-Boixereu, N., Estrada, M., Gasol, J.M., 1999.
832 Bacterioplankton and phytoplankton biomass and production during summer
833 stratification in the northwestern Mediterranean Sea. *Deep Sea Res. Part I Oceanogr.*
834 *Res. Pap.* 46, 985–1019.

835 Peled, Y., Zemah Shamir, S., Shechter, M., Rahav, E., Israel, A., 2018. A new perspective on
836 valuating marine climate regulation: The Israeli Mediterranean as a case study. *Ecosyst.*

837 Serv. 29, 83–90. <https://doi.org/10.1016/j.ecoser.2017.12.001>

838 Pinardi, N., Masetti, E., 2000. Variability of the large scale general circulation of the
839 Mediterranean Sea from observations and modelling: a review. Palaeogeogr.
840 Palaeoclimatol. Palaeoecol. 158, 153–173. [https://doi.org/10.1016/S0031-0182\(00\)00048-1](https://doi.org/10.1016/S0031-0182(00)00048-1)

841 Psarra, S., Tselepides, A., Ignatiades, L., 2000. Primary productivity in the oligotrophic
842 Cretan Sea (NE Mediterranean): seasonal and interannual variability. Prog. Oceanogr.
843 46, 187–204.

844 Rahav, E., Belkin, N., Paytan, A., Herut, B., 2018. Phytoplankton and bacterial response to
845 desert dust deposition in the coastal waters of the southeastern Mediterranean Sea: A
846 four-year in situ survey. Atmosphere (Basel). 9. <https://doi.org/10.3390/atmos9080305>

847 Rahav, E., Herut, B., Levi, A., Mulholland, M.R., Berman-Frank, I., 2013. Springtime
848 contribution of dinitrogen fixation to primary production across the Mediterranean Sea.
849 Ocean Sci. 9, 489–498.

850 Rahav, Eyal, Herut, B., Stambler, N., Bar-Zeev, E., Mulholland, M.R., Berman-Frank, I.,
851 2013. Uncoupling between dinitrogen fixation and primary productivity in the eastern
852 Mediterranean Sea. J. Geophys. Res. Biogeosciences 118, 195–202.

853 Rahav, E., Paytan, A., Mescioglu, E., Bar-Zeev, E., Martínez Ruiz, F., Xian, P., Herut, B.,
854 2020. Bio-Aerosols Negatively Affect Prochlorococcus in Oligotrophic Aerosol-Rich
855 Marine Regions. Atmosphere (Basel). 11, 540.

856 Rahav, E., Silverman, J., Raveh, O., Hazan, O., Rubin-Blum, M., Zeri, C., Gogou, A., Kralj,
857 M., Pavlidou, A., Kress, N., 2019. The deep water of Eastern Mediterranean Sea is a
858 hotspot for bacterial activity. Deep. Res. Part II Top. Stud. Oceanogr. 164, 135–143.
859 <https://doi.org/10.1016/j.dsr2.2019.03.004>

860 Raveh, O., David, N., Rilov, G., Rahav, E., 2015. The temporal dynamics of coastal

862 phytoplankton and bacterioplankton in the eastern mediterranean sea. PLoS One 10,
863 e0140690. <https://doi.org/10.1371/journal.pone.0140690>

864 Redfield, A.C., 1934. On the proportions of organic derivatives in sea water and their relation
865 to the composition of plankton. University Press of Liverpool Liverpool.

866 Robarts, R.D., Zohary, T., Waisser, M.J., Yacobi, Y.Z., 1996. Bacterial abundance, biomass,
867 and production in relation to phytoplankton biomass in the levantine basin of the
868 southeastern Mediterranean Sea. Mar. Ecol. Prog. Ser. 137, 273–281.
869 <https://doi.org/10.3354/meps137273>

870 Rosenberg, D.R., Haber, M., Goldford, J., Lalzar, M., Aharonovich, D., Al-Ashhab, A.,
871 Lehahn, Y., Krom, M.D., Segrè, D., Steindler, L., Sher, D., 2020. Particle-associated
872 and free-living bacterial communities in an oligotrophic sea are affected by different
873 environmental and anthropogenic factors. bioRxiv 2020.04.20.051391.
874 <https://doi.org/10.1101/2020.04.20.051391>

875 Roth-Rosenberg, D., Aharonovich, D., Luzzatto-Knaan, T., Vogts, A., Zoccarato, L.,
876 Eigemann, F., Nago, N., Grossart, H.P., Voss, M., Sher, D., 2020. Prochlorococcus cells
877 rely on microbial interactions rather than on chlorotic resting stages to survive long-term
878 nutrient starvation. MBio 11, 1–13. <https://doi.org/10.1128/mBio.01846-20>

879 Santinelli, C., 2015. DOC in the Mediterranean Sea, in: Biogeochemistry of Marine
880 Dissolved Organic Matter. Elsevier, pp. 579–608.

881 Shaked, Y., Genin, A., 2017. Eilat IUI monitoring NMP Report 2017.

882 Simon, M., Azam, F., 1989. Protein content and protein synthesis rates of planktonic marine
883 bacteria. Mar. Ecol. Prog. Ser. 51, 201–213. <https://doi.org/10.3354/meps051201>

884 Siokou-Frangou, I., Bianchi, M., Christaki, U., Christou, E.D., Giannakourou, A., Gotsis, O.,
885 Ignatiades, L., Pagou, K., Pitta, P., Psarra, S., 2002. Carbon flow in the planktonic food
886 web along a gradient of oligotrophy in the Aegean Sea (Mediterranean Sea). J. Mar.

887 Syst. 33, 335–353.

888 Siokou-Frangou, I., Christaki, U., Mazzocchi, M.G., Montresor, M., Ribera D’Alcala, M.,

889 Vaque, D., Zingone, A., 2010. Plankton in the open mediterranean Sea: A review.

890 Biogeosciences 7, 1543–1586. <https://doi.org/10.5194/bg-7-1543-2010>

891 Sisma-Ventura, G., Kress, N., Silverman, J., Gertner, Y., Ozer, T., Biton, E., Lazar, A.,

892 Gertman, I., Rahav, E., Herut, B., 2021. Post-eastern Mediterranean Transient Oxygen

893 Decline in the Deep Waters of the Southeast Mediterranean Sea Supports Weakening of

894 Ventilation Rates. Front. Mar. Sci. 7. <https://doi.org/10.3389/fmars.2020.598686>

895 Steinberg, D.K., Carlson, C.A., Bates, N.R., Johnson, R.J., Michaels, A.F., Knap, A.H., 2001.

896 Overview of the US JGOFS Bermuda Atlantic Time-series Study (BATS): a decade-

897 scale look at ocean biology and biogeochemistry. Deep Sea Res. Part II Top. Stud.

898 Oceanogr. 48, 1405–1447. [https://doi.org/10.1016/S0967-0645\(00\)00148-X](https://doi.org/10.1016/S0967-0645(00)00148-X)

899 Tanaka, T., Zohary, T., Krom, M.D., Law, C.S., Pitta, P., Psarra, S., Rassoulzadegan, F.,

900 Thingstad, T.F., Tselepidis, A., Woodward, E.M.S., Flaten, G.A.F., Skjoldal, E.F.,

901 Zodiatis, G., 2007. Microbial community structure and function in the Levantine Basin

902 of the eastern Mediterranean. Deep Sea Res. Part I Oceanogr. Res. Pap. 54, 1721–1743.

903 <https://doi.org/10.1016/j.dsr.2007.06.008>

904 Thingstad, T.F., Krom, M.D., Mantoura, R.F.C., Flaten, G.A.F., Groom, S., Herut, B., Kress,

905 N., Law, C.S., Pasternak, A., Pitta, P., 2005. Nature of phosphorus limitation in the

906 ultraoligotrophic eastern Mediterranean. Science (80-.). 309, 1068–1071.

907 Tillmann, U., 1998. Phagotrophy by a plastidic haptophyte, *Prymnesium patelliferum*. Aquat.

908 Microb. Ecol. 14, 155–160.

909 Unrein, F., Gasol, J.M., Not, F., Forn, I., Massana, R., 2014. Mixotrophic haptophytes are

910 key bacterial grazers in oligotrophic coastal waters. ISME J. 8, 164–176.

911 van den Engh, G.J., Doggett, J.K., Thompson, A.W., Doblin, M.A., Gimpel, C.N.G., Karl,

912 D.M., 2017. Dynamics of Prochlorococcus and Synechococcus at station ALOHA
913 revealed through flow cytometry and high-resolution vertical sampling. *Front. Mar. Sci.*
914 4, 1–14. <https://doi.org/10.3389/fmars.2017.00359>

915 Van Wambeke, F., Christaki, U., Bianchi, M., Psarros, S., Tselepides, A., 2000. Heterotrophic
916 bacterial production in the Cretan Sea (NE Mediterranean). *Prog. Oceanogr.* 46, 205–
917 216.

918 Van Wambeke, F., Lefèvre, D., Prieur, L., Sempéré, R., Bianchi, M., Oubelkheir, K.,
919 Bruyant, F., 2004. Distribution of microbial biomass, production, respiration, dissolved
920 organic carbon and factors controlling bacterial production across a geostrophic front
921 (Almeria-Oran, SW Mediterranean Sea). *Mar. Ecol. Prog. Ser.* 269, 1–15.

922 Vidussi, F., Marty, J.-C.C., Chiavérini, J., 2000. Phytoplankton pigment variations during the
923 transition from spring bloom to oligotrophy in the northwestern Mediterranean Sea.
924 *Deep Sea Res. Part I Oceanogr. Res. Pap.* 47, 423–445. [https://doi.org/10.1016/S0967-0637\(99\)00097-7](https://doi.org/10.1016/S0967-0637(99)00097-7)

926 Viviani, D.A., Church, M.J., 2017. Decoupling between bacterial production and primary
927 production over multiple time scales in the North Pacific Subtropical Gyre. *Deep Sea
928 Res. Part I Oceanogr. Res. Pap.* 121, 132–142.

929 Viviani, D.A., Karl, D.M., Church, M.J., 2015. Variability in photosynthetic production of
930 dissolved and particulate organic carbon in the North Pacific Subtropical Gyre. *Front.
931 Mar. Sci.* 2, 73.

932 Wambeke, F., Christaki, U., Giannakourou, A., Moutin, T., Souvmerzoglou, K., 2002.
933 Longitudinal and vertical trends of bacterial limitation by phosphorus and carbon in the
934 Mediterranean Sea. *Microb. Ecol.* 43, 119–133.

935 Yacobi, Y.Z., Zohary, T., Kress, N., Hecht, A., Robarts, R.D., Waisser, M., Wood, A.M., Li,
936 W.K.W., 1995. Chlorophyll distribution throughout the southeastern Mediterranean in

937 relation to the physical structure of the water mass. *J. Mar. Syst.* 6, 179–190.

938 [https://doi.org/10.1016/0924-7963\(94\)00028-A](https://doi.org/10.1016/0924-7963(94)00028-A)

939 Yelton, A.P., Acinas, S.G., Sunagawa, S., Bork, P., Pedrós-Alió, C., Chisholm, S.W., 2016.

940 Global genetic capacity for mixotrophy in marine picocyanobacteria. *ISME J.* 10, 2946–

941 2957. <https://doi.org/10.1038/ismej.2016.64>

942 Yoge, T., Rahav, E., Bar-Zeev, E., Man-Aharonovich, D., Stambler, N., Kress, N., Béjà, O.,

943 Mulholland, M.R., Herut, B., Berman-Frank, I., 2011. Is dinitrogen fixation significant

944 in the Levantine Basin, east Mediterranean Sea? *Environ. Microbiol.* 13, 854–871.

945 Zervoudaki, S., Christou, E.D., Nielsen, T.G., Siokou-Frangou, I., Assimakopoulou, G.,

946 Giannakourou, A., Maar, M., Pagou, K., Krasakopoulou, E., Christaki, U., 2007. The

947 importance of small-sized copepods in a frontal area of the Aegean Sea. *J. Plankton Res.*

948 29, 317–338.

949 Zohary, T., Herut, B., Krom, M.D., Mantoura, R.F.C., Pitta, P., Psarra, S., Rassoulzadegan,

950 F., Stambler, N., Tanaka, T., Thingstad, T.F., 2005. P-limited bacteria but N and P co-

951 limited phytoplankton in the Eastern Mediterranean—a microcosm experiment. *Deep*

952 *Sea Res. Part II Top. Stud. Oceanogr.* 52, 3011–3023.

953